LICENTIATE THESIS

Development of Constituents for Multi-functional Composites Reinforced with Cellulosic Fibers

Zainab Al-Maqdasi

Polymeric Composite Materials

LULEÅ UNIVERSITY OF TECHNOLOGY

Development of Constituents for Multi-functional Composites Reinforced with Cellulosic Fibers

LICENTIATE THESIS

By

Zainab Al-Maqdasi

Division of Materials Science
Department of Engineering Sciences and Mathematics
Luleå University of Technology
Luleå, Sweden
SE 97187

Supervisors
Prof. Roberts Joffe; Prof. Nazanin Emami; and Dr. Liva Pupure

Printed by Luleå University of Technology, Graphic Production 2019

ISSN 1402-1757
ISBN 978-91-7790-372-7 (print)
ISBN 978-91-7790-373-4 (pdf)

Luleå 2019

www.ltu.se

Anyone who isn't embarrassed of who they were last year probably isn't learning enough.

Alain de Botton

I would say …who they were 'last week'

Abstract

Bio-based composites are being increasingly used in applications where weight saving, and environmental friendliness are as important as structural performance. Obviously, bio-based materials have their limitations regarding durability and stability of the properties, but their potential in use for advanced applications can be expanded if they were functionalized and considered beyond their structural performance.

Multifunctionality in composites can be achieved by modifying either of the composite constituents at different levels so that they can perform energy-associated roles besides their structural reinforcement in the system. For the fibers, this can be done at the microscale by altering their microstructure during spinning process, or by applying functional coatings. As for the matrix, it is usually done by incorporating particles that can impart the required characteristics to the matrix. The nano-sized particles that might be considered for this objective are graphene derivatives and carbon nanotubes. A big challenge with such materials is the difficulty to reach the homogeneous dispersion and stable network necessary for them to become functional. However, once the network is formed, the composite can have improved mechanical performance together with one or more of the added functionalities such as barrier capabilities, thermal and/or electrical conductivities or electromagnetic interference shielding effectiveness.

Enormous work has been done to achieve the functionality in composites produced with special care in laboratories. However, when it comes to mass production, it is both cost and energy inefficient to use intricate, complex methods for the manufacturing. Hence there is a need to investigate the potential of using scalable and industrial-relevant techniques and materials with acceptable compromise between cost and performance, in order to meet the modern technology's need in a sustainable manner.

The work presented in this thesis aims at achieving functional composites based on natural and man-made cellulosic fibers suitable for industrial upscaling. Conductive Regenerated Cellulose Fibers (RCFs) were produced by coating them with copper by electroless plating process using commercial materials. On the other hand,

commercial masterbatches based on Graphene Nano-Platelets (GNPs) were used to produce wood polymer composites (WPC) with added functionality by melt extrusion process. The process is one of the conventional methods used in polymer production and needs no modifications for processing functional composites. Both materials together can be used to produce hybrid multiscale functional composites.

The incorporation of the GNP into a matrix of high-density polyethylene (HDPE) has resulted in improvement in the mechanical properties of the polymer as well as composite reinforced by wood flour. Stiffness has increased significantly while effect of modifiers on the strength was less pronounced (>100% and 18% for stiffness and strength at 15 wt% GNP loading). Besides, enhancement of thermal conductivity at high graphene loadings was observed. Moreover, time-dependent response of the polymer has also been affected and the addition of GNP has resulted in reduced viscoplastic strains and improved creep behavior.

The copper-coated cellulose fibers showed a substantial increase in electrical conductivity (measured resistance was <1Ω/50 mm of coated samples) and a potential in use as sensor materials. However, these results come with the cost of reduction in mechanical properties of fibers (10% and 70% for tensile stiffness and strength, respectively), due to the effect of chemicals involved in the process.

Keywords: Composites, cellulosic fibers, modified matrix, nanocomposites, graphene nanoplatelets, wood polymer composites, functionality, mechanical performance.

Preface

The work presented in this thesis was performed at Luleå University of Technology (Luleå, Sweden) with a close collaboration with RISE SICOMP (Piteå, Sweden). Part of the work has been funded by European Union and region Norbotten within the framework of Interreg-Nord projects (granted project Smart-WPC). This funding is highly appreciated and acknowledged. The Swedish Foundation for International Cooperation in Research and Higher Education, STINT, is also acknowledged for the support of COndective REgenerated CEllulose fibers (CORECE) project. Research financial support of the excellence and innovation area of Smart Machine and Materials (SMM) at Luleå University of Technology is highly accredited.

The thesis is a result of the hard work, fruitful discussions and wise visions of many people without whom it could not have existed. First and foremost, I would like to express my unlimited gratitude to my main supervisor, Professor Joffe, for sharing the knowledge, the continuous support and the wisdom in directing the work. Your 'always-available' for the small as well as bigger problems has facilitated the smooth flow of the work.

My gratitude is extended to my co-supervisors prof. Emami and Dr. Pupure, who have been more than professional support. Thank you for pushing me forwards… Prof. Emami, I always count on you for shaping the independent researcher in me.

Students I supervised/co-supervised during the first half of my journey (Astrid, Diego, Lena and Vanessa), you didn't only help acquiring results with patience and motivation but also gave me the chance to share the knowledge I received once when I was in your place. We also learned a lot together!

Colleagues in the division of Material Science; groupmates of polymeric composite materials; colleagues at SICOMP, especially Guan; and my co-authors – Thank you for providing the unique working adventure. I look forward to more collaborations.

I would never imagine the long way I came through without the special people in my life who have been my rigid wall to lean on during tough times. My family (close and extended), my dearest nieces who always know the way to paint a smile on my face, my friends and the closest of them here in Luleå – Members of the WA group 'cool girls-extended'; thank you for all the real and virtual cups of caffeinated drinks we had together.

I'm in debt for the rest of my life to the one and only person who suffered the real consequences of my choices and faced them with respect and understanding - My husband, true friend and partner, Ali. Always … to the moon and back!

Luleå, Spring 2019
Zainab Al-Maqdasi

List of Appended Papers

Paper I

Zainab Al-Maqdasi, Abdelghani Hajlane, Abdelghani Renbi, Ayoub Ouarga, Shailesh Singh Chouhan and Roberts Joffe.

Conductive Regenerated Cellulose Fibers (RCFs) by Electroless Plating.

Published in: Fibers 2019, Volume 7, Issue 38

Paper II

Zainab Al-Maqdasi, Guan Gong, Birgitha Nyström, Nazanin Emami, Roberts Joffe.

Characterization of wood and Graphene Nanoplatelets (GNPs) Reinforced Polymer Composites.

To be submitted to: Polymer Testing

Paper III

Liva Pupure, Zainab Al-Maqdasi, Guan Gong, Nazanin Emami, Roberts Joffe.

Effect of Nano-reinforcement on the Time-dependent Properties of Graphene Modified High Density Polyethylene.

To be submitted to: Journal of Thermoplastic Composite Materials

Other Contributions

Guan Gong, Birgitha Nyström, Zainab Al-Maqdasi, Roberts Joffe and Runar Långström.

Development of Functionalized Wood Composites for Smart Products

Extended abstract submitted and presented in conference: Flow Processes During Composites Manufacturing – 14, 2018, Luleå (2 pages)

Zainab Al-Maqdasi, Guan Gong, Birgitha Nyström, and Roberts Joffe.

Wood Fiber Composites with Added Multi-functionality

Conference paper and poster presentation at 18th European Conference on Composite Materials (ECCM 18), 2018, Athens (8 pages)

Zainab Al-Maqdasi, Liva Pupure, Nazanin Emami and Roberts Joffe.

Time Dependent Properties of Graphene reinforced HDPE

Extended abstract submitted and accepted for poster presentation at: 9th International Conference on Composites Testing and Model Identification (COMPTEST), 2019, Luleå (2 pages)

Zainab Al-Maqdasi, Nazanin Emami, Roberts Joffe, Shailesh S. Chouhan, Ayoub Ouarga, and Abdelghani Hajlane.

Development of Reliable Copper Coating Procedure of Regenerated Cellulose Fibers for Enhanced Conductivity

Extended abstract submitted and accepted for full paper and oral presentation at: Twenty- second International Conference on Composite Materials (ICCM22), 2019, Melbourne.

Contents

1. Introduction

1.1. Composites – short overview

Composite materials are those composed of at least two-phase components of distinctive physical characteristics, combined to form a new material possessing properties that individual constituents cannot provide [1]. Usually, one phase is in a discontinuous form (fibrous, particulate, platelets, etc.) while the other is in a form of continuous matrix whose role is to keep together the fibers and ensures a smooth and efficient transformation of the loads between the constituents. The most common type of composites used in industry nowadays are the fiber reinforced polymer composites. Both classes of polymers, thermoplastics and thermosets, ranging from commodity plastics to epoxies and engineering plastics are being reinforced with various types of fibers, such as glass, carbon, polymer fibers (e.g. polyethylene and aramid fibers), or natural fibers.

The advantages of these materials lie in their light weight and the tunable properties to the direction of load application. Reduction in mass of a structural part made of aluminum reaches up to 20% if replaced by thermoplastic composite of the same performance [2].

The performance of the final composite depends on several factors beside the choice of material and reinforcement form. Wetting of fibers and subsequently adhesion between the constituents is one of the most effective parameters on load transfer capability of the composite. The manufacturing process and processing parameters are other important factors. Defects induced in the composite during manufacturing (damage or misalignment of the fibers or presence of voids) limit the exploitation of the composite's full potential.

Composite technology has developed from the basic solutions for construction applications to the most advanced applications in aerospace and advanced electronics. Figure 1 shows the state of market of fiber reinforced polymer composites in a recent year where automotive industry is in the leading position with respect to the application of composites. Processing and manufacturing have also evolved from the

simple hand lay up to the use of additive manufacturing techniques where more complex geometries are possible to produce by implementing computer aided designs e.g. in 3D printing [3].

Due to the growing awareness in environment, attention has been shifted to bio-based composites and their potential to replace conventional fossil fuel-based counterparts. Those can be in a form of bio-based matrix, example polylactide (PLA) [4] or starch; bio-based fibers such as mineral, plant or animal based fibers; or all natural composites [5,6]. Plant fibers, more specifically cellulosic fibers, and their composites are the central focus of this study and will further be discussed in the sequel.

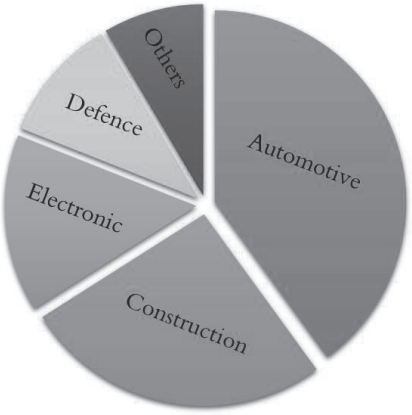

Figure 1. Global fiber reinforced polymer composite market by application, 2016. Figure recreated from [7].

1.2. Cellulose Fibers

Cellulose is the most abundant polymer on earth and the main component in plant fibers. It is available from variety of sources and used in different applications. Figure 2 shows some of the common sources of cellulose and some other alternative ones. As most of cellulose fibers are extracted from plants, they are subject to variation in properties due to the dependence of their composition on the growing/cultivation conditions. Textile industry of cellulose fibers accounted for 44% of the global

revenue share in 2015, driven by fabric reinforced polymer composites as their major application [8]. This is result of the ambitious attempt to replace some of the most conventional manmade fibers (e.g. glass) by bio-based fibers in wider applications. When compared to glass fibers, they compete in many important aspects, as shown in Table 1, mostly related to energy and environment. Among the various types of cellulose fibers, flax, hemp and soft-wood-kraft possess the closest mechanical properties to glass fibers [10], especially stiffness wise. Young's modulus and strength of soft wood fibers are about 1000 MPa and 40 GPa respectively, compared to 2000–3500 MPa and 70.0 GPa for glass E. The values are comparable if properties are normalized with densities (1.5 g/cm^3 for soft wood vs 2.5 g/cm^3 for glass). However, they are inferior in terms of environmental durability and compatibility with the polymer matrix and need surface modifications (chemical, thermal, etc.) to improve fiber/matrix interface. Almost all discussions about the performance of the cellulose fibers in their composites involve the constituents' interaction and degree of adhesion. For example, in studying general performance [11,12] or a specific property such as resistance to creep [13]. Improving the adhesion by the chemical modification of fiber surface has largely been investigated by the use of different chemicals [11,14] some of which have shown negative impact on the aspect ratio of fibers [15].

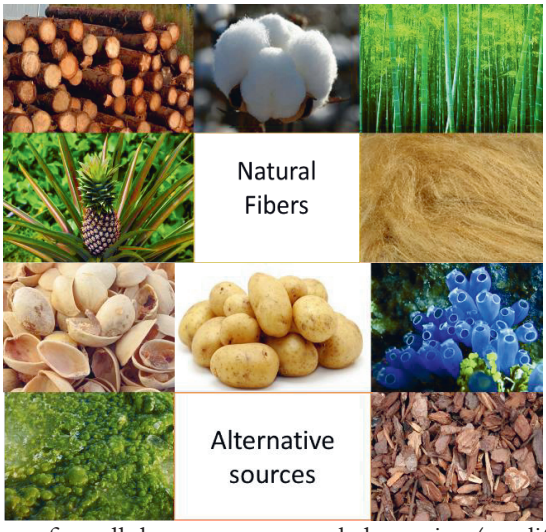

Figure 2. Sources for cellulose, common and alternative (modified from [16]).

Table 1. Comparison between natural fibers and glass fibers (recreated from [9]).

	Natural Fibers (NF)	Glass Fibers
Density	Low	~2× that of NF
Cost	Low	Low, but higher than NF
Renewability	Yes	No
Recyclability	Yes	No
Energy consumption	Low*	High
Distribution	Wide	Wide
CO2 neutral	Yes*	No
Abrasion to machines	No	Yes
Health risk when inhaled	No	Yes
Disposal	Biodegradable	Not biodegradable

* depending on the harvest and processing

1.2.1. Regenerated Cellulose Fibers (RCFs)

Cellulose by itself has an identical structure regardless the variation of its sources [17]. If cellulose molecules are extracted and shaped into continuous fibrous form, more stable properties can be achieved, compared to the wide range offered by natural fibers. Fibers produced by this concept are known as the regenerated cellulose fibers (RCFs). Extraction and regeneration of cellulose is done by different methods, some of which involve hazardous chemicals and solvents, making the low environmental impact of these fibers questionable, despite their natural resources. However, production technologies of these materials are progressing, and some newer generations and modifications of these fibers are assessed to have better environmental impact than cotton fibers for instance – let alone if compared to conventional fossil based fibers [18].

A general description of the processing of RCFs, extracted from the website of the manufacturer of viscose rayon cord CORDENKA® [19], is described here:

The process starts with the use of high purity pulp which goes through multi-stage processing to produce multi-filament yarn. Carbon disulfide and sodium hydroxide are used to dissolve the pulp. The solution goes through stages of ripening, filtration, degassing, and then spinning. Through spinnerets, the viscose is pumped into a spinning bath where cellulose yarn regenerates and precipitates. These yarns are then

stretched, fixated and washed before wound on bobbins. In this stage, the yarn is ready to get the appropriate sizing after washing and let to dry. To improve sustainability of the process, the spinning bath is reproduced, and chemicals are recovered to be reused. Example specifications of the resulted fiber yarns, available under the trade name CORDENKA® Super 3, are reported in Table 2.

Table 2. Properties of commercial RCF yarn CORDENKA® 700 Super 3 (extracted from [20]).

Number of filaments (nominal)	Linear density (g/m)	Breaking force (N)	Breaking tenacity (kN · m/kg)	Elongation at break (%)
1350	2.485	127.9	515	12.2

Properties of fibers are dependent on the type of the processing method and its parameters. Variation can be in terms of physical characteristics like shape of fibers (as presented in Figure 3 left) or in terms of performance (Figure 3 right). Reported elastic moduli of some of these fibers range between 9.4 and 41.7 GPa for regular viscose and Bocell, respectively. However, high properties are usually associated to fibers carefully produced in the laboratory, as in the case of the mentioned Bocell fibers, which is not commercialized [21].

Studies on manmade cellulosic fibers compared to natural fibers showed that the former have better influence on the strength of PLA composite compared to natural fibers while marginal effect on stiffness was noticed. On the other hand, bonding between the fibers and the matrix seems to be better in natural fibers that have a rough surface compared to that of RCFs [22]. Based on their processing technologies, the reinforcing efficiency of RCFs in composites vary, and thus properties can be tuned to the needs by the fiber-type selection [23]. One very important characteristic of the composites based on these fibers is the improved energy absorption and elongation at break inherent from their high stretch ability [24,25].

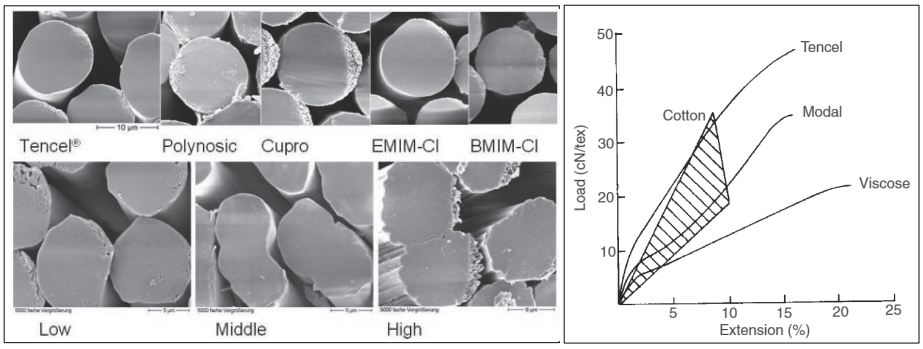

Figure 3. (left): Variation of the cross section of RCF with production method (upper; scale bar is 10 μm), and with variation of parameters of the same process; in this case the concentration of acid in the spinning bath (lower; scale bar is 5 μm). Image adapted from [26]; (right): properties of RCF produced in different methods.

1.3. Wood Polymer Composites

Wood polymer composite (WPC) is termed for the composites with any type of wood reinforcement (wood fibers, wood flour, etc.) in a polymer matrix (thermoplastic or thermoset) [1]. The most commonly used matrix, though, is thermoplastic, more specifically those of low processing temperature (mostly polyolefins). This is due to the thermal instability of wood (and most natural fibers) over 200 ºC, leading polyolefins with melting points below 180 °C to be the matrix of choice [27], and extrusion to be the processing method when producing WPC. However, the matrix is not merely limited to thermoplastic, and research on thermoset-wood composites is available as well [28] but the role of wood in such composites is limited to being a cost-reducing filler rather than reinforcement. In fact, commercial products of wood thermoset polymers exist since as early as 1916 in the gearshift knob of Rolls Royce [29].

The general classification of synthetic polymers in terms of thermal processing places polyolefins (polymers having at least one unsaturated carbon-carbon double bonds) in the class of thermoplastic polymers that can be reformed and reshaped after their production by the effect of heat. Classification based on production volume and consumption, ranks them first among other polymers [30] which makes them interesting materials for low cost, moderate performance applications. Among the

widely used polyolefins in applications of composites are polyethylene (PE) in its different varieties (low density (LDPE), high density (HDPE), linear low density (LLDPE) and ultrahigh molecular weight (UHMWPE)), and polypropylene (PP) [31]. Similar to the development of other types of composites, reinforcement of polyolefins ranges from the conventional fibers [32] including polyolefin fibers themselves [33], going through natural and bio-based fibers [34] to the most recent trend of reinforcement at the nanoscale using organic and inorganic nanofillers [35]. These polymers are known for the semi-crystalline nature and improved crystallinity results in large improvement in their mechanical properties. Partially, crystallinity is affected by the production of the polymer that influences directly the arrangement of the polymer chains. Branched, low molecular weight polymers exhibit lower degrees of crystallinity due the bulky arrangement of the branches that prevents the formation of highly ordered folded chains segments within the molecular structure. The opposite is true for the polymers with high molecular weight long chains with limited branches. Improving crystallinity has been practiced by the addition of nucleating agents in terms of additives around which polymer crystals initiate and grow [36].

The availability of wood from side streams of forest industry makes it a good candidate for low cost- high throughput production composites. Due to the high content of cellulose in wood, apparent physical characteristics, machining and use of WPC are similar to those of pure wood [37] with the advantage of reduced maintenance. Additionally, the use of thermoplastic polymer increases the sustainability of these materials by offering recyclability and reusability after disposal. This might come with the cost of possible collapsing of the wood cell walls as can be seen in Figure 4 which are the source of their mechanical performance. However, available studies show the reversed effect on performance after multiple processing might be noticed and it is attributed to the possible improvement in dispersion of wood in the matrix, or the enhancement in the molecular structure of the polymer [38]. Since higher performing grades of WPCs are based on fossil-derived-polymers, the biodegradability is obviously negatively influenced.

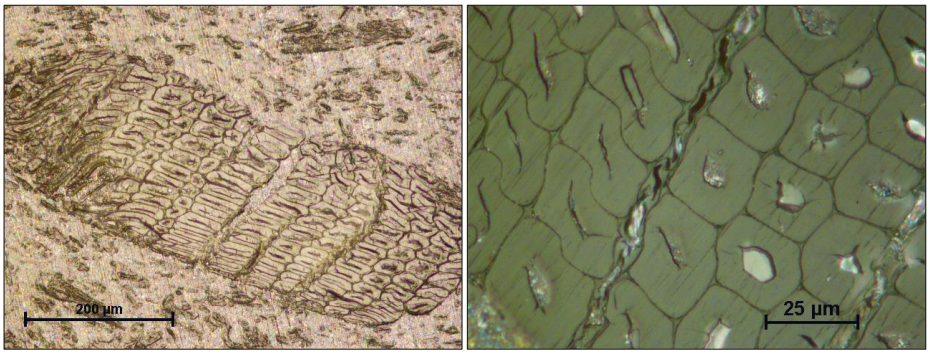

Figure 4. Micrograph of cross section of wood chip in polymer matrix after processing by melt compounding followed by compression molding. Left image shows the collapsed fibers and in the right image is a close up showing some of the normal-looking wood fibers and other collapsed ones.

Thermal stability, environmental durability as well as long term performance are some of the properties that define the application of polymers in general. Current applications of WPC vary but are limited to low end use applications such as building and construction, furniture, automotive interiors, and other consumer goods such as packaging.

In addition to the two main components in WPCs (wood and polymer), additives such as compatibilizers, UV stabilizers, fire retardants, pigments and others, are usually added for improved performance. This is facilitated by the flexibility of the processing method of WPCs. More recently, additives in the nano-scale are gaining increased interest in the research of this materials for their potential reinforcing effect or improving the durability of composite. Mechanical properties of the WPC were improved by about 300% by the addition of single wall CNT and MAPE as a coupling agent together with the enhanced dimensional stability and moisture uptake resistance [39]. It was found that these particles occupy the voids in the materials restricting water from penetrating in. The improved adhesion between the matrix and reinforcement is an additional factor for improved water uptake resistance. The incorporation of the inorganic nanoclay and TiO_2 has been found to modify the thermal stability, UV resistance and moisture uptake resistance of the WPC from polymer blends and enhanced the processing and the miscibility of the blends [40]. Similar findings were reported in literature [41–43] and reviewed in [44].

1.4. Multifunctionality

Despite the efforts exerted to promote sustainable technologies, the report of Union of Concerned Scientists on Global warming [45] states that the earth has reached a no-return point in the amount of CO_2 concentrations in the atmosphere in 2016, most of which is the human input as fossil fuel emissions. Therefore, more attention is needed to cut-off the human impact on the environment and increase the efforts towards achieving more sustainable world and preserve the natural resources. Changing energy sources to green energy is continually increasing in many countries and in many sectors [46] but more is still required. Material reusability and recyclability are additional routes towards that goal. Moreover, the trend has been shifted during recent years towards taking the material development to a new level by introducing multifunctionality [47]. The concept of multifunctionality is represented by the ability of the material to perform more than one role, leading to the reduction in the number of components in a product and, consequently, to saving more weight and reducing energy consumption. Beside the structural reinforcement, the additional role in a multifunctional system is usually energy-associated (Figure 5).

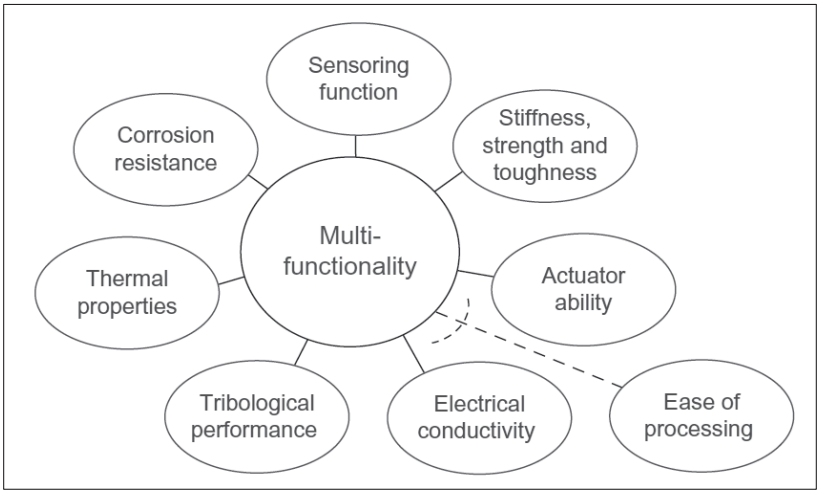

Figure 5. Schematic of possible combinations for multifunctional systems. Figure adopted from [48].

1.4.1. Routes for Multifunctional Composites

Composites are ideal systems for the added functionality, thanks to the way they are constructed that allows for wide range of possible modifications. Chemical or physical enhancement to any of the constituents, addition of functional constituents or hybridization and producing sandwich structures are examples for these possibilities. Some of the possible routes to functionalize composites are viewed next. Although the concept of multifunctional composite material is still relatively new, it has been applied to quite advanced applications such as electronics and sensing applications by the use of conventional composites [48]. Applying this knowledge to natural fiber composite, though, is still challenging and offers room for improvement.

Essential for the understanding of multifunctionality and how it is achieved, is it to be familiar with the term 'percolation threshold'. It can be defined as the extent of modification necessary to change the state of material/system from 'lacking' to 'gaining' a certain property. This happens when the material has built a network within the structure, that has at least one connected path capable of efficient energy transfer (in its different forms) from one end to the other, (Figure 6). However, there is no single value equivalent to this term since it is system- and property dependent. There are, basically, three commonly used percolation threshold variants: thermal, electrical and rheological.

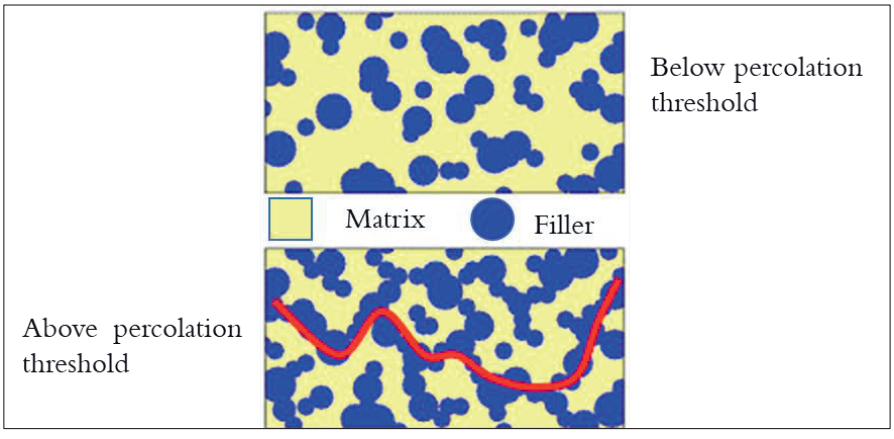

Figure 6. Schematic showing the principle of Percolation threshold. Image recreated from [49].

Functional fibers

The use of fibers that have the desired functionality as intrinsic property (such as metallic fibers) is the straight forward method in the direction of imparting their characteristics to the host system. However, some limitations of weight, size or incompatibility, generated the need to induce the characteristics on fibers originally lacking them. This can be done by modifications at different levels, some of which are presented in Figure 7. The choice of fiber form (long/short/woven) or the functionalization technique has an essential effect on the result. For example, the physical deposition of functional particles on the surface of continuous long fibers eases the formation of the connected network and reduces the percolation threshold (Figure 7a). Other techniques represented by permanent alteration of the structure of fibers (grafting of molecules on the surface) or changing the internal composition (spinning the fibers from solution containing functional particles) are shown in Figure 7b & c, respectively. However, degree of complexity and efficiency for upscaling of the methods are factors to be considered.

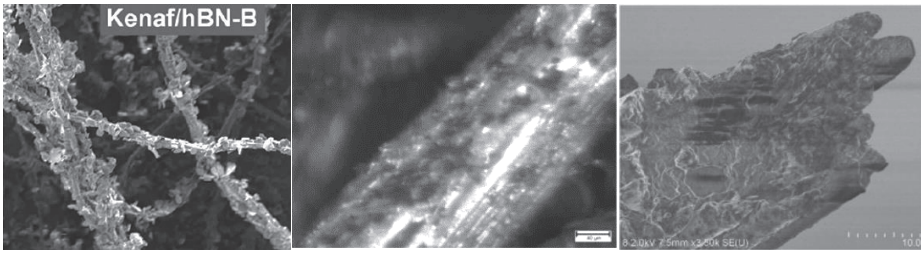

Figure 7. Functionalized fibers by various means; left: absorption on surface [50], center: surface chemical modification [51], right: internal molecular structure modification [52].

Functional matrix

Similar to fibers, the use of polymers having intrinsic functional property, individually or in form of blends (chemical/physical) is possible. Example for functional polymers are the polyanilines which have good electrical conductivity. However, these are usually unstable polymers and lose their conductivity upon oxidation, they are also difficult to process [53] compared to conventional polymers. Then multifunctionality

by modifying the matrix of the composite becomes mostly correlated to the addition of functional additives (mostly at the nanoscale) to the microscopic reinforced composites [54]. This also results in increasing the value and competitiveness of the polymeric composites with other structural materials [48]. In general, it is observed that the enhancement in properties occurs upon the addition of very low loading of nano-scale particles especially into thermosetting matrix, mediated by their initial liquid state that result in well dispersed secondary phase.

Several additives have been reported that can be used to impart functionality by modifying the polymer matrix. Some of these are metallic particles, ceramic particles, inorganic clays, and carbon-derived additives. The latter are the most interesting among all due to their remarkable specific properties and their ability to improve the performance of composites without compromising the weight. They can provide more than one functionality if the added amount is enough to overcome the percolation threshold for these functionalities.

Carbon allotropes in the nano-scale can be realized based on their dimensionality into: 0-D represented by the fullerenes, 1-D as for the carbon nanotubes, 2-D for the graphene sheets, and 3-D as for the bulk carbon black or the graphite multi-layered sheets or diamond. A close look at those allotropes as presented in Figure 8, one can realize that they are all formed from the single layer graphene sheet by folding and wrapping, making graphene an interesting material to study and characterize [55,56]. Graphene is a continuous lattice of hexagonal rings of carbon atoms bonded covalently in the SP^2 hybridization configuration with one atom in the thickness direction. With tensile modulus as high as 1TPa, intrinsic strength of 130 GPa and a thermal and electrical conductivities up to 3000-5000 W/m K [57] and 6000 S/cm [58], respectively, graphene is superior to all other materials known to date.

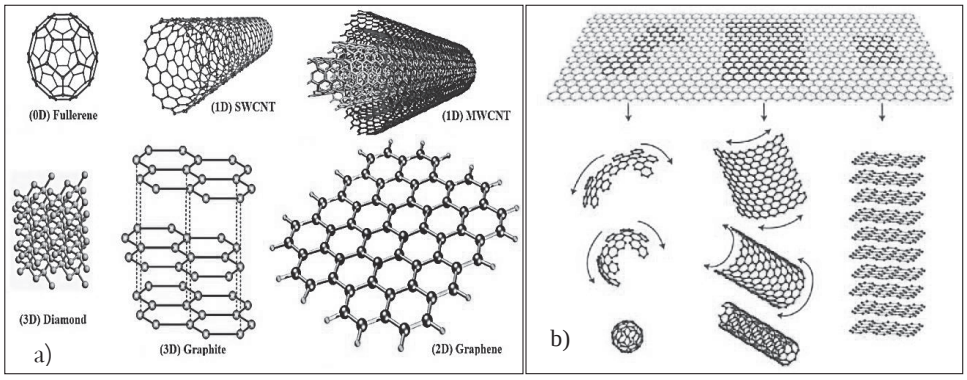

Figure 8. a) Dimensionality of carbon allotropes [55], b) Graphene as the basic for all graphitic forms [59].

For long time, carbon nanotubes were dominating the research and many studies have been conducted to report the effect of adding them in different amounts on the mechanical and physical properties of the composites. However, major challenges were faced regarding the dispersion and the costly production of these materials. Graphene synthesis is much easier and more naturally produced by thermal exfoliation of the abundant matter graphite [60]. Moreover, studies have shown that at same filler loading, the impact of graphene on the mechanical properties is more pronounced than those achieved with CNTs [61], due to the larger contact area.

The performance of the polymer nanocomposite is affected by the degree of nanofiller dispersion and the strength of the interfacial bonding between the polymer and the particles. These are the most critical factors to achieve improvement of properties of the nanocomposites and they depend strongly on the processing technique used for their production. Three main techniques have been realized for the production of the polymer nanocomposites; namely **in situ polymerization**, **solution mixing** and **melt blending** [62]. The first two are common for thermoplastics and thermosets while the last is for the production of thermoplastic nanocomposites. Pre-treatment (chemical or mechanical) of the nanofillers is required for some of these techniques to ensure their homogeneous dispersion in the polymer and prevent re-aggregation. Resulting nanocomposites are suitable for further processing by conventional techniques like injection and compression molding, thermoforming and blow molding [63]. The in situ polymerization method involves

sonication of the nanofiller in the monomer or its solution prior to its thermal polymerization, and the process might involve different catalysts or chemicals [64]. Continuous increase in the viscosity of the produced polymer accompanies the reaction until final solid product is produced. Polymers that are thermally unstable or insoluble in solutions can be efficiently prepared by this technique. In the solution mixing process, separate solutions of nanofillers and the polymers are prepared, and the nanocomposite is formed by mixing, followed by evaporation of the two solutions to recover the nanocomposite. For the nanofiller to be well dispersed in the polymer, the solution is agitated rigorously to overcome the hydrogen bonding causing the agglomeration. In the melt compounding process, shear forces are utilized to disperse the nanofillers in the viscous polymer melt. The technique is considered to be environmentally friendly and suitable for most polyolefin polymers with moderate molecular weight since it profits of the conventional industrial equipment such as single or twin-screw extruders. Functionalization of the nanofillers play a significant role in enhancing their dispersion in the polymer matrix despite the type of processing technique followed.

1.4.2. Functionalities Expected in Graphene Doped Composites

Thermal conductivity

Heat conduction in polymers occurs essentially by phonon vibration mechanism. The amorphous nature of the polymers and the structural defects are therefore responsible factors for dissipation of thermal energy by scattering the phonons rendering them thermal insulators with conductivity in the range of 0.5-1 W/m K [65]. This value is far from the good conductivity of copper (400 W/m K) carried by the free electrons. Graphene has the combined mechanisms of heat conduction which makes it a very high conductive material with values reaching as high as 5000 W/m K even though the contribution of electrons is smaller than phonons. Inclusion of graphene in polymers results in a complex mechanism for heat transfer since the large surface area of graphene sheets in contact with the polymer chains acts as phonon scattering points. The improved thermal conductivity of the graphene-polymer systems thus is mostly a result of a continuous network of graphene particles dispersed throughout

the polymer. This property is subject to the influence of directionality of graphene sheets in the polymer. Thermal conductivity of polymers reinforced with graphene increased with increasing loading and number of layers of graphene sheet (anisotropic improvement) [65] while better mechanical properties can be achieved by the better exfoliation and higher aspect ratio (less layers). Not only the performing properties are affected but also more efficient production of the polymer part can be achieved when incorporating conductive additives due to the reduced time, and consequently the production cost [66]. Figure 9 shows the change in mechanism of thermal wave transport through the polymer by the effect of doping with aligned and networked thermal conductive particles.

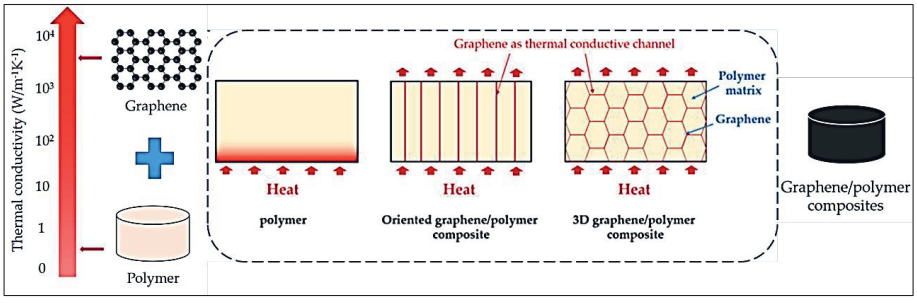

Figure 9. Mechanism for improving thermal conductivity of polymers by addition of graphene. Figure recreated from [65].

Electrical conductivity

Except for the rare type of electrically conductive polymers such as earlier mentioned anilines, most polymers are insulators, which is the reason why plastics are used to insulate cables. Polymers have a resistivity in the order of magnitude of 10^{16} Ωm, compared to that of best conductors (metals) which are in the order of magnitude of 10^{-8} Ωm. However, introducing high conductive additives such as graphene (electrical conductivity of graphene sheets prepared by hydrogen arc discharge is reported to be 2×10^{3} S/cm [67]) can change this property over the percolation threshold. Electrical conductivity is dominated by the electron transfer in the material and controlled by the well-known Ohm's law $R=V/I$.

Figure 10 shows a schematic of how the amount of graphene in the polymer matrix would change the mechanism of the electrical conductance. At the percolation threshold the electron transport is achieved by the tunneling effect where graphene sheets are close enough to but not necessarily touching to allow it, thus the electrical conductance is defined by the distance separating the conductive particles. After the percolation threshold, the electrical conductivity is achieved through end-to-end path of the graphene sheets which makes the composite a more efficient conductor.

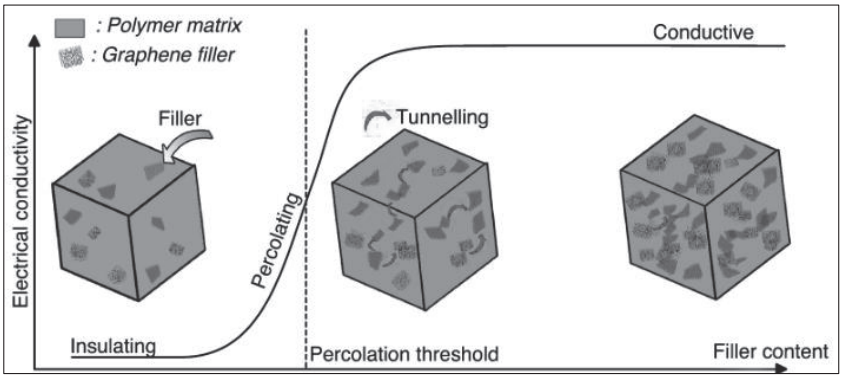

Figure 10. Formation of graphene network to overcome electrical percolation. Adopted from [68].

Several factors affect the resulted conductivity of composite systems, some of which are listed below [69]:

- Conductivity of the constituents
- Moisture content
- Chemical composition (especially C/O ratio)
- The interconnection of the additives which is dictated by their shape and amount
- Processing method; which can also affect some of the abovementioned factors (e.g. interconnection and composition).

Electromagnetic Interference (EMI) Shielding

The importance of this property comes from the hazardous effect of conducting/radiating electromagnetic (EM) signals to the living organisms, or the disturbance to the electronics in the range of their effectiveness. The mode of travel and the characteristic of frequency of the electromagnetic interference (EMI) waves are the criteria by which these waves are classified. The shielding effectiveness is the ratio between the magnitude of the incident electric or magnetic field in non-shielded materials to that of the shielded (i.e. attenuation). While some techniques to improve this property involve surface finishing and post fabrication processes, others consider permanent modification. Example of the former is coating, which is subject to wear, fading, peeling or environmental erosion. Permanent modification involves functionalization of composite constituents or production of hybrid composites. The shielding mechanism is represented either by the efficiency of the additive to absorb, reflect EM waves or both [53]. Similar factors to those affecting the electrical conductivity can affect this property. Due to the mentioned intrinsic properties of graphene, it is considered as a promising additive to shielding polymers against EM radiation without compromising the weight. The heat conductance of graphene can help dissipate the heat resulting from the attenuation and render graphene composites dual or multifunctional systems as demonstrated in Figure 11.

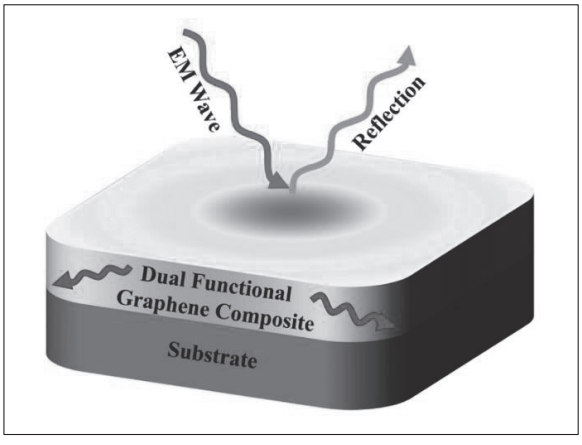

Figure 11. The dual action of graphene in blocking EM radiation and dissipating heat. Image source: Physics World.

Barrier properties

The mechanism for providing the composite with barrier characteristics is similar against most external particles. Barrier can shield against certain gas molecules, water molecules etc. by providing torturous routes that prevent or delay the molecular diffusion (see Figure 12). For this reason, it is understandable that additives in the platelets form make better barriers when compared to single or fewer layers additives.

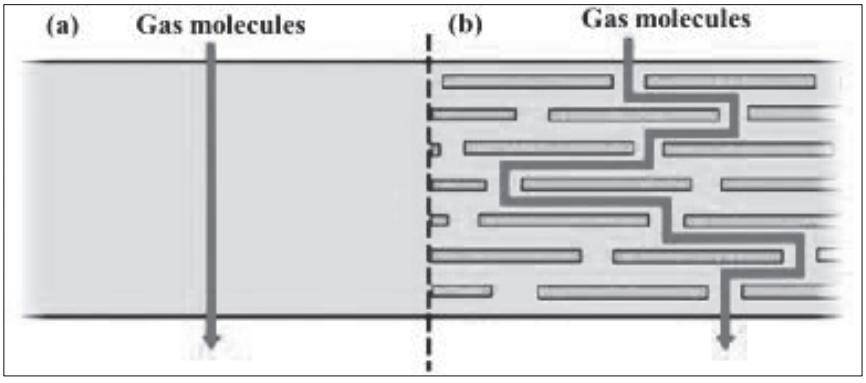

Figure 12. Formation of torturous path against molecules. [70].

Fire retardancy is regarded as barrier property by blocking the oxygen molecules from reaching the burning surface. Among other carbonaceous additives to (Carbon Black, Carbon nanotubes, Extended Graphite, etc.) polypropylene system, graphene was found to be the most efficient fire retardant [35] and this property is dependent on graphene's degree of exfoliation. Graphene is considered as environmentally friendly non-halogenated flame retardant. However, the incompatibility of the nano sheets with the matrix material might result in longer dripping times than those experienced by the conventional retardants [71].

Other Investigated Properties

Researchers have investigated the effect of addition of graphene on wide range of material properties. Some of these are presented here only to show the potential with no further discussion:

- Supercapacitance [72]

- Crystallinity and thermal stability [73,74]
- Time-dependent properties [75]
- Machinability [76]
- Tribological properties (scratch and wear resistance and friction enhancement) [77] as self-lubricated solids.
- Biodegradability of polymers [78].
- Energy harvesting and saving [79] and more.

1.4.3. Selected Examples for Multifunctional Carbon-based Composites

Summarized below are some of the examples and their references for the added functionalities achieved by incorporating nano-particles in the composite, together with the percentages of changes.

ref	*Materials*	*Primary property*	*~% change*	*Secondary property*	*Remarks*
[80]	HDPE/GNP	Degradation temp. (at which 2% mass loss occurs)	52	Thermal conductivity (44% increase compared to neat HDPE)	Addition of 5 wt% GNP having lateral size of 25μm
[81]	PP/CB PP/MWCNT PP/TRGO PP/MLG	***E, σ*** $_{yield}$ ***E, σ*** $_{yield}$ ***E, σ*** $_{yield}$ ***E, σ*** $_{yield}$	4.7, -1.5 7.1, 0 34, 2.6 20, -3	Flame retardancy: Peak heat release rate (PHRR) change -62 % -57 % -74 % -71 %	Other flame-retardency related properties were also investigated e.g. oxygen index (OI), anti-dripping behavior, Time to Ignition (TTI), onset decomposition temperature, etc.
[82]	EP/FLG	***K*** (thermal conductivity)	3500	EMI shielding: blocking 99.99% high frequency EM radiation	Very high graphene loading 50 wt%. But lower content also investigated in the same ref.
[58]	Styrene Butadiene Rubber SBR/GNP	***E*** ***σ, σ*** $_{tear}$	782 413, 709	Electrical conductivity (3 times higher than neat polymer)	Addition of 16.7 vol% GNPs. Composite prepared by solution mixing
[83]	PLA/GNP	***E*** ***σ***	27 6.3	Temperature sensitive shape recovery of 91% vs 81% for neat PLA	Addition of 3 wt% surface modified GNP

2. Current Work

2.1. Motivation

In 2017, a research project (Smart-WPC) within the framework of Interreg Nord projects funded by European Union and region Norrbotten was initiated between Luleå University of Technology (LTU), Rise SICOMP (previously Swerea SICOMP) and Centria University of Applied Sciences in Finland. The goal is to develop materials and technologies that allow the use of bio-based materials in more advanced applications and high-end products. Such step would increase the value of raw materials from forest industry and reduce waste of natural resources. For instance, electrically conductive WPC boards can be used as advanced decking materials with de-icing/anti-icing characteristics. Scratch resistant materials with EMI shielding properties are suitable for production of electronic casings from environmentally friendly sources.

From the literature survey, similar work using graphene rather than carbon nanotubes is lacking. Therefore, outcomes of the project will enrich the research field with more fundamental studies on graphene and its potential.

In parallel, an initiative collaboration project (CORECE by STINT) between LTU and Mohammed VI Polytechnic University in Morocco was established with the aim of developing functional cellulosic fibers for use in damage detecting and electronic application. These fibers can also be used in combination with multi-functional WPC to develop hybrid materials with even more functionalities and better properties.

The project 'smart materials' was supporting both these investigations aiming to link the knowledge from the multifunctional materials to multifunctional systems.

The overall outcome of the work is in line with the pursuit of sustainability in resources and industries.

2.2. Methodology

The work presented in this thesis aims at the development of new material systems and designs; therefore, until now main activities were focused on collection and analysis of experimental data. This also includes optimization of processing parameters, material composition and morphology to achieve desired properties of composites. However, modelling of properties is also carried out to predict some of the properties of studied materials as well as for validation of applicability and accuracy of existing analytical models.

2.3. Summary of Papers

In view of the advances presented in the previous chapter and the motivation of the work, the first stage to achieving the research goals is by investigating ways of functionalizing the individual composite constituents. In **Paper I**, commercial regenerated cellulose fibers have been coated with copper from commercial packages using electroless plating process. Both the material selection and the processing technique are suitable for upscaling to produce e.g. functional textiles. The copper was successfully deposited on the surface of the fibers and electrical conductivity increased significantly. On the other hand, sensitivity of fibers to chemicals resulted in a reduction in their mechanical performance to a large degree as was shown from the values of tensile strength and modulus. Such preliminary assessment of the approach reveals the need to investigate further possibilities to minimize the damage. **Paper II** presents the experimental characterization after modification of the polymer matrix with two types of reinforcement. Materials available in the market rather than produced in the laboratory were used together with conventional production techniques. Results show that even though the size of the incorporated graphene nanoplatelets is far from being in the 'supposedly' nano-scale, they resulted in significant improvement in the mechanical properties of the composites and increased their thermal conductivity and dimensional stability. The fewer graphene layers and

the higher graphene content are two factors responsible for the maximum improvement achieved.

After characterizing the material for static short-term performance and the efficiency of the nano-reinforcement to enhance the overall properties, interest arises to investigate how they would perform on the long term. **Paper III** deals with the time-dependent properties of polymers modified with nano-platelets. Effect of the addition of different amounts of these platelets on the viscoplastic and viscoelastic strains of the composites was investigated. Identification of model parameters and validation of its applicability to predict the behavior of these materials have also been performed. Results showed that high content of platelets (15 wt%) in the composites impacted the creep behavior positively and resulted in decrease in viscoplastic and viscoelastic strains.

3. Future work

The following is planned as future work; either as a continuation of data collection by means of further comprehensive characterization for better understanding of material behavior; or as new routes for constituents' functionalization. The ultimate goal is to investigate the properties of functionalized hybrid composites.

Fibers

- Investigate the interfacial bonding between RCF/copper and copper/matrix together with their possible damage detection characteristics in composites.
- Use of different route/material to coat RCFs seeking their conductivity. This is already in progress by depositing CNTs on the surface of fibers.

Matrix

- Investigation of the additional properties such as the tribological properties.
- Study and comparison of different material grades on the desired properties. Characterization of the new composite based on linear low-density polyethylene (LLDPE) is in progress.

Hybrid Composite

- Production and characterization of the composite made of hybrid hierarchical structure of the modified constituents.

References

[1] B.D. Agarwal, L.J. Broutman, K. Chandrashekhara, Analysis and performance of fiber composites, Third Edit, Wiley, 2006.

[2] BASF Automotive Solutions, Look Out Aluminum, Thermoplastic Composites Can Reduce More Mass, (2015). https://automotive.basf.com/news/read/look-aluminum-thermoplastic-composites-can-reduce-mass (accessed April 17, 2019).

[3] L.G. Blok, M.L. Longana, H. Yu, B.K.S. Woods, An investigation into 3D printing of fibre reinforced thermoplastic composites, Addit. Manuf. (2018). doi:10.1016/j.addma.2018.04.039.

[4] L. Pupure, J. Varna, R. Joffe, F. Berthold, A. Miettinen, Mechanical properties of natural fiber composites produced using dynamic sheet former, Wood Mater. Sci. Eng. (2018). doi:10.1080/17480272.2018.1482368.

[5] R. Joffe, B. Madsen, K. Nättinen, A. Miettinen, Strength of cellulosic fiber/starch acetate composites with variable fiber and plasticizer content, J. Compos. Mater. (2015). doi:10.1177/0021998314528734.

[6] M.A. Dweib, B. Hu, A. O'Donnell, H.W. Shenton, R.P. Wool, All natural composite sandwich beams for structural applications, Compos. Struct. (2004). doi:10.1016/S0263-8223(03)00143-0.

[7] Grand View Research, Fiber Reinforced Polymer (FRP) Composites Market Analysis By Fiber Type (Glass, Carbon, Basalt, Aramid), By Application (Automotive, Construction, Electronic, Defense), By Region, And Segment Forecasts, 2018 - 2025, 2017.

[8] Grand View Research, Cellulose Fiber Market Analysis By Product Type (Natural, Synthetic), By Application (Textile, Hygiene, Industrial), By Regions (North America, Asia Pacific, Europe, Central & South America, Middle East & Africa), And Segment Forecasts, 2018 - 2025, 2016.

[9] P. Wambua, J. Ivens, I. Verpoest, Natural fibres: Can they replace glass in fibre reinforced plastics?, Compos. Sci. Technol. 63 (2003) 1259–1264. doi:10.1016/S0266-3538(03)00096-4.

[10] A.K. Bledzki, J. Gassan, Composites reinforced with cellulose based fibres, Prog. Polym. Sci. (1999). doi:10.1016/S0079-6700(98)00018-5.

[11] T.-J. Chung, J.-W. Park, H.-J. Lee, H.-J. Kwon, H.-J. Kim, Y.-K. Lee, W. Tai Yin Tze, The Improvement of Mechanical Properties, Thermal Stability, and Water Absorption Resistance of an Eco-Friendly PLA/Kenaf Biocomposite Using Acetylation, Appl. Sci. (2018). doi:10.3390/app8030376.

[12] N.S. Yatigala, D.S. Bajwa, S.G. Bajwa, Compatibilization improves physico-mechanical properties of biodegradable biobased polymer composites, Compos. Part A Appl. Sci. Manuf. (2018).

doi:10.1016/j.compositesa.2018.01.011.

[13] J. Gassan, A.K. Bledzki, Influence of fiber surface treatment on the creep behavior of jute fiber-reinforced polypropylene, J. Thermoplast. Compos. Mater. (1999). doi:10.1177/089270579901200504.

[14] J. Chen, Y. Wang, C. Gu, J. Liu, Y. Liu, M. Li, Y. Lu, Enhancement of the mechanical properties of basalt fiber-wood-plastic composites via maleic anhydride grafted high-density polyethylene (MAPE) addition, Materials (Basel). 6 (2013) 2483–2496. doi:10.3390/ma6062483.

[15] P.J. Herrera-Franco, A. Valadez-González, A study of the mechanical properties of short natural-fiber reinforced composites, Compos. Part B Eng. (2005). doi:10.1016/j.compositesb.2005.04.001.

[16] D.R. Shankaran, Cellulose Nanocrystals for Health Care Applications, in: Appl. Nanomater., 2018. doi:10.1016/b978-0-08-101971-9.00015-6.

[17] K. Jedvert, T. Heinze, Cellulose modification and shaping – a review, J. Polym. Eng. (2017). doi:10.1515/polyeng-2016-0272.

[18] L. Shen, M.K. Patel, Life Cycle Assessment of Man-made Cellulose Fibers, Lenzinger Berichte LIFE. (2010).

[19] Cordenka GmbH & Co KG, (n.d.). http://www.cordenka.com/en/the_company_cordenka/production/rayon-production-process/ (accessed April 20, 2019).

[20] B.H. den Ambtman, Profile of premium rayon reinforcement for high performance tires, Chem. Fibers Int. (2002).

[21] H. Santamala, R. Livingston, H. Sixta, M. Hummel, M. Skrifvars, O. Saarela, Advantages of regenerated cellulose fibres as compared to flax fibres in the processability and mechanical performance of thermoset composites, Compos. Part A Appl. Sci. Manuf. 84 (2016) 377–385. doi:10.1016/j.compositesa.2016.02.011.

[22] A.K. Bledzki, A. Jaszkiewicz, D. Scherzer, Mechanical properties of PLA composites with man-made cellulose and abaca fibres, Compos. Part A Appl. Sci. Manuf. 40 (2009) 404–412. doi:10.1016/j.compositesa.2009.01.002.

[23] J. Ganster, H.P. Fink, Novel cellulose fibre reinforced thermoplastic materials, Cellulose. (2006). doi:10.1007/s10570-005-9045-9.

[24] C. Kahl, M. Feldmann, P. Sälzer, H.P. Heim, Advanced short fiber composites with hybrid reinforcement and selective fiber-matrix-adhesion based on polypropylene – Characterization of mechanical properties and fiber orientation using high-resolution X-ray tomography, Compos. Part A Appl. Sci. Manuf. (2018). doi:10.1016/j.compositesa.2018.05.014.

[25] J.C. Zarges, D. Minkley, M. Feldmann, H.P. Heim, Fracture toughness of injection molded, man-made cellulose fiber reinforced polypropylene, Compos. Part A Appl. Sci. Manuf. (2017).

doi:10.1016/j.compositesa.2017.03.022.

[26] T. Roder, J. Moosbauer, G. Kliba, S. Schlader, G. Zuckerstatter, H. Sixta, Compartaive Characterisation of man-made regenerated cellulose fibres, Lenzinger Berichte. 87 (2009) 98–105.

[27] D.J. Gardner, Y. Han, L. Wang, Wood–Plastic Composite Technology, Curr. For. Reports. 1 (2015) 139–150. doi:10.1007/s40725-015-0016-6.

[28] R. Nouwezem, M.E. Borredon, A. Gaset, Production and properties of thermosetting composites based on wood and unsaturated- polyester mixtures, Bioresour. Technol. (1994). doi:10.1016/0960-8524(94)90129-5.

[29] C.M. Clemons, R.M. Rowell, D. Plackett, B.K. Segerholm, Wood/nonwood thermoplastic composites, in: Handb. Wood Chem. Wood Compos. Second Ed., 2012. doi:10.1201/b12487.

[30] D. Nwabunma, Overview of Polyolefin Composites, in: Polyolefin Compos., 2007. doi:10.1002/9780470199039.ch1.

[31] N.J. Al-Thani, J. Bhadra, K.M. Zadeh, Polyolefin Composites and Nanocomposites, in: Polyolefin Compd. Mater., Springer, Cham, 2015: pp. 157–179. doi:10.1007/978-3-319-25982-6_6.

[32] G.D. SIMS, W.R. BROUGHTON, Glass Fiber Reinforced Plastics—Properties, Compr. Compos. Mater. (2000) 151–197. doi:10.1016/B0-08-042993-9/00181-9.

[33] M. Mosleh, N.P. Suh, J. Arinez, Manufacture and properties of a polyethylene homocomposite, Compos. Part A Appl. Sci. Manuf. (1998). doi:10.1016/S1359-835X(97)00122-X.

[34] C. Vasile, R.N. Darie-Niţă, E. Părpăriţă, Performance of biomass filled polyolefin composites, in: Biocomposites Des. Mech. Perform., 2015. doi:10.1016/B978-1-78242-373-7.00012-3.

[35] S. Coiai, E. Passaglia, A. Pucci, G. Ruggeri, Nanocomposites based on thermoplastic polymers and functional nanofiller for sensor applications, Materials (Basel). (2015). doi:10.3390/ma8063377.

[36] J. Qiao, M. Guo, L. Wang, D. Liu, X. Zhang, L. Yu, W. Song, Y. Liu, Recent advances in polyolefin technology, Polym. Chem. 2 (2011) 1611. doi:10.1039/c0py00352b.

[37] M. Niaounakis, Building and Construction Applications, in: Biopolym. Appl. Trends, 2015. doi:10.1016/b978-0-323-35399-1.00010-7.

[38] D. Kurniawan, B.S. Kim, H.Y. Lee, J.Y. Lim, Effects of repetitive processing, wood content, and coupling agent on the mechanical, thermal, and water absorption properties of wood/polypropylene green composites, in: J. Adhes. Sci. Technol., 2013. doi:10.1080/01694243.2012.695948.

[39] H.Y. Kordkheili, M. Farsi, Z. Rezazadeh, Physical, mechanical and

morphological properties of polymer composites manufactured from carbon nanotubes and wood flour, Compos. Part B Eng. 44 (2013) 750–755. doi:10.1016/j.compositesb.2012.04.023.

[40] B.K. Deka, T.K. Maji, Effect of TiO 2 and nanoclay on the properties of wood polymer nanocomposite, Compos. Part A Appl. Sci. Manuf. 42 (2011) 2117–2125. doi:10.1016/j.compositesa.2011.09.023.

[41] C. Guo, L. Zhou, J. Lv, Effects of expandable graphite and modified ammonium polyphosphate on the flame-retardant and mechanical properties of wood flour-polypropylene composites, Polym. Polym. Compos. 21 (2013) 449–456. doi:10.1002/app.

[42] Y. Lei, Q. Wu, C.M. Clemons, F. Yao, Y. Xu, Influence of nanoclay on properties of HDPE/wood composites, J. Appl. Polym. Sci. 106 (2007) 3958–3966. doi:10.1002/app.27048.

[43] S. Sheshmani, A. Ashori, M. Arab Fashapoyeh, Wood plastic composite using graphene nanoplatelets, Int. J. Biol. Macromol. 58 (2013) 1–6. doi:10.1016/j.ijbiomac.2013.03.047.

[44] M. Hetzer, D. De Kee, Wood/polymer/nanoclay composites, environmentally friendly sustainable technology: A review, Chem. Eng. Res. Des. 86 (2008) 1083–1093. doi:10.1016/j.cherd.2008.05.003.

[45] U. of C. Scientists, How Do We Know that Humans Are the Major Cause of Global Warming?, Www.Ucsusa.Org. (2017).

[46] K. Ek, Public and private attitudes towards "green" electricity: The case of Swedish wind power, Energy Policy. 33 (2005) 1677–1689. doi:10.1016/j.enpol.2004.02.005.

[47] J.A. Balta, F. Bosia, V. Michaud, G. Dunkel, J. Botsis, J.-A. Månson, Smart composites with embedded shape memory alloy actuators and fibre Bragg grating sensors: Activation and control, Smart Mater. Struct. 14 (2005) 457–465. doi:10.1088/0964-1726/14/4/001.

[48] K. Friedrich, Multifunctionality of Polymer Composites Challenges and New Solutions, 2015.

[49] M.C. Simulation, The Effects of Uniaxial Strain on the Percolation Threshold of Fibers in Polymer Composites through Monte Carlo Simulation, University of Toronto, 2014.

[50] C. Xia, A.C. Garcia, S.Q. Shi, Y. Qiu, N. Warner, Y. Wu, L. Cai, H.R. Rizvi, N.A. D'Souza, X. Nie, Hybrid boron nitride-natural fiber composites for enhanced thermal conductivity, Sci. Rep. 6 (2016) 1–8. doi:10.1038/srep34726.

[51] F.G. Souza, G.E. Oliveira, C.H.M. Rodrigues, B.G. Soares, M. Nele, J.C. Pinto, Natural brazilian amazonic (curauá) Fibers modified with polyaniline nanoparticles, Macromol. Mater. Eng. 294 (2009) 484–491.

doi:10.1002/mame.200900033.

[52] M. Tian, L. Qu, X. Zhang, K. Zhang, S. Zhu, X. Guo, G. Han, X. Tang, Y. Sun, Enhanced mechanical and thermal properties of regenerated cellulose/graphene composite fibers, Carbohydr. Polym. 111 (2014) 456–462. doi:10.1016/j.carbpol.2014.05.016.

[53] D.D.L. Chung, Electromagnetic interference shielding effectiveness of carbon materials, Carbon N. Y. (2001). doi:10.1016/S0008-6223(00)00184-6.

[54] C. González, J.J. Vilatela, J.M. Molina-Aldareguía, C.S. Lopes, J. LLorca, Structural composites for multifunctional applications: Current challenges and future trends, Prog. Mater. Sci. 89 (2017) 194–251. doi:10.1016/j.pmatsci.2017.04.005.

[55] N.F. Atta, A. Galal, E.H. El-Ads, Graphene — A Platform for Sensor and Biosensor Applications, in: Biosens. - Micro Nanoscale Appl., 2015: pp. 38–84. doi:10.5772/60676.

[56] C.N.R. Rao, A.K. Sood, K.S. Subrahmanyam, A. Govindaraj, Graphene: The new two-dimensional nanomaterial, Angew. Chemie - Int. Ed. 48 (2009) 7752–7777. doi:10.1002/anie.200901678.

[57] M.J. Nine, M.A. Cole, D.N.H. Tran, D. Losic, Graphene: a multipurpose material for protective coatings, J. Mater. Chem. A. 3 (2015) 12580–12602. doi:10.1039/C5TA01010A.

[58] S. Araby, Q. Meng, L. Zhang, H. Kang, P. Majewski, Y. Tang, J. Ma, Electrically and thermally conductive elastomer/graphene nanocomposites by solution mixing, Polym. (United Kingdom). 55 (2014) 201–210. doi:10.1016/j.polymer.2013.11.032.

[59] A.K. Geim, K.S. Novoselov, The rise of graphene., Nat. Mater. (2007). doi:10.1038/nmat1849.

[60] J. Kim, J. Kim, B.S. Yim, J.M. Kim, The effects of functionalized graphene nanosheets on the thermal and mechanical properties of epoxy composites for anisotropic conductive adhesives (ACAs), Microelectron. Reliab. (2012). doi:10.1016/j.microrel.2011.11.002.

[61] M. El Achaby, A. Qaiss, Processing and properties of polyethylene reinforced by graphene nanosheets and carbon nanotubes, Mater. Des. 44 (2013) 81–89. doi:10.1016/j.matdes.2012.07.065.

[62] S.N. Tripathi, G.S.S. Rao, A.B. Mathur, R. Jasra, Polyolefin/graphene nanocomposites: a review, RSC Adv. 7 (2017) 23615–23632. doi:10.1039/C6RA28392F.

[63] W.S. Khan, N.N. Hamadneh, W.A. Khan, Polymer nanocomposites – synthesis techniques, classification and properties, in: P. Di Sia (Ed.), Sci. Appl. Tailored Nanostructures, One Central Press, 2015: p. 376.

[64] C. Park, Z. Ounaies, K.A. Watson, R.E. Crooks, J. Smith, S.E. Lowther, J.W.

Connell, E.J. Siochi, J.S. Harrison, T.L. St Clair, Dispersion of single wall carbon nanotubes by in situ polymerization under sonication, Chem. Phys. Lett. 364 (2002) 303–308. doi:10.1016/S0009-2614(02)01326-X.

[65] A. Li, C. Zhang, Y.F. Zhang, Thermal conductivity of graphene-polymer composites: Mechanisms, properties, and applications, Polymers (Basel). 9 (2017) 1–17. doi:10.3390/polym9090437.

[66] R. Rothon, C. DeArmitt, Fillers (Including Fiber Reinforcements), in: Brydson's Plast. Mater. Eighth Ed., Butterworth-Heinemann, 2016: pp. 169–204. doi:10.1016/B978-0-323-35824-8.00008-6.

[67] Z.S. Wu, W. Ren, L. Gao, J. Zhao, Z. Chen, B. Liu, D. Tang, B. Yu, C. Jiang, H.M. Cheng, Synthesis of graphene sheets with high electrical conductivity and good thermal stability by hydrogen arc discharge exfoliation, ACS Nano. (2009). doi:10.1021/nn900020u.

[68] A.J. Marsden, D.G. Papageorgiou, C. Vallés, A. Liscio, V. Palermo, M.A. Bissett, R.J. Young, I.A. Kinloch, Electrical percolation in graphene-polymer composites, 2D Mater. (2018). doi:10.1088/2053-1583/aac055.

[69] D. Pathania, D. Singh, A review on electrical properties of fiber reinforced polymer composites, Int. J. Theor. Appl. Sci. 1 (2009) 34–37.

[70] Y. Cui, S.I. Kundalwal, S. Kumar, Gas barrier performance of graphene/polymer nanocomposites, Carbon N. Y. (2016). doi:10.1016/j.carbon.2015.11.018.

[71] P. Khalili, K.Y. Tshai, I. Kong, C.H. Yeoh, K.E. Materials, The Effects of Graphene and Flame Retardants on Flammability and Mechanical Properties of Natural Fibre Reinforced Polymer Composites, Key Eng. Mater. 701 (2016) 286–290. doi:10.4028/www.scientific.net/KEM.701.286.

[72] A. Ramadoss, B. Saravanakumar, S.J. Kim, Thermally reduced graphene oxide-coated fabrics for flexible supercapacitors and self-powered systems, Nano Energy. 15 (2015) 587–597. doi:10.1016/j.nanoen.2015.05.009.

[73] P. Xu, X. Luo, Y. Zhou, Y. Yang, Y. Ding, Enhanced cold crystallization and dielectric polarization of PLA composites induced by P[MPEGMA-IL] and graphene, Thermochim. Acta. 657 (2017) 156–162. doi:10.1016/j.tca.2017.10.005.

[74] R. Valapa, S. Hussain, P.K. Iyer, G. Pugazhenthi, V. Katiyar, Influence of graphene on thermal degradation and crystallization kinetics behaviour of poly(lactic acid), J. Polym. Res. 22 (2015). doi:10.1007/s10965-015-0823-2.

[75] A. Vieira, V.C. Pinto, A. Pinto, F.D. Magalhaes, Viscoplastic model analysis about the influence of graphene reinforcement in poly (lactic acid) time-dependent mechanical behaviour, Int. J. Automot. Compos. (2015). doi:10.1504/ijautoc.2015.070568.

[76] V. Sridharan, T. Raja, N. Muthukrishnan, Study of the Effect of Matrix, Fibre

Treatment and Graphene on Delamination by Drilling Jute/Epoxy Nanohybrid Composite, Arab. J. Sci. Eng. 41 (2016) 1883–1894. doi:10.1007/s13369-015-2005-2.

[77] D. Berman, A. Erdemir, A. V. Sumant, Graphene: A new emerging lubricant, Mater. Today. (2014). doi:10.1016/j.mattod.2013.12.003.

[78] V. Sridhar, I. Lee, H.H. Chun, H. Park, Graphene reinforced biodegradable poly(3-hydroxybutyrate-co-4-hydroxybutyrate) nano-composites, Express Polym. Lett. 7 (2013) 320–328. doi:10.3144/expresspolymlett.2013.29.

[79] K.K. Sadasivuni, D. Ponnamma, J. Kim, S. Thomas, Graphene-based polymer nanocomposites in electronics, Graphene-Based Polym. Nanocomposites Electron. (2015) 1–382. doi:10.1007/978-3-319-13875-6.

[80] E. Tarani, Z. Terzopoulou, D.N. Bikiaris, T. Kyratsi, K. Chrissafis, G. Vourlias, Thermal conductivity and degradation behavior of HDPE/graphene nanocomposites: Pyrolysis, kinetics and mechanism, J. Therm. Anal. Calorim. 129 (2017) 1715–1726. doi:10.1007/s10973-017-6342-0.

[81] B. Dittrich, K.A. Wartig, D. Hofmann, R. Mülhaupt, B. Schartel, Flame retardancy through carbon nanomaterials: Carbon black, multiwall nanotubes, expanded graphite, multi-layer graphene and graphene in polypropylene, Polym. Degrad. Stab. 98 (2013) 1495–1505. doi:10.1016/j.polymdegradstab.2013.04.009.

[82] F. Kargar, Z. Barani, M. Balinskiy, A.S. Magana, J.S. Lewis, A.A. Balandin, Dual-Functional Graphene Composites for Electromagnetic Shielding and Thermal Management, Adv. Electron. Mater. 5 (2019) 1800558. doi:10.1002/aelm.201800558.

[83] M. Keramati, I. Ghasemi, M. Karrabi, H. Azizi, M. Sabzi, Incorporation of surface modified graphene nanoplatelets for development of shape memory PLA nanocomposite, Fibers Polym. 17 (2016) 1062–1068. doi:10.1007/s12221-016-6329-7.

Paper I

Conductive Regenerated Cellulose Fibers (RCFs) by Electroless Plating

Zainab Al-Maqdasi, Abdelghani Hajlane, Abdelghani Renbi, Ayoub Ouarga, Shailesh Singh Chouhan, and Roberts Joffe

Reformatted version of paper originally published in ***Fibers*** **2019,7, 38**

Digital Object Identifier (DOI): **https://doi.org/10.3390/fib7050038**

Communication

Conductive Regenerated Cellulose Fibers (RCFs) by Electroless Plating

Zainab Al-Maqdasi[1], Abdelghani Hajlane[2], Abdelghani Renbi[1], Ayoub Ouarga[2], Shailesh Singh Chouhan[1] and Roberts Joffe[1]

[1] Luleå University of Technology, Luleå, 97187, Sweden
[2] Mohammed VI Polytechnic University, Benguerir, 43150, Morocco

Abstract

Continuous metalized regenerated cellulose fibers for advanced applications (e.g., multi-functional composites) are produced by electroless copper plating. Copper is successfully deposited on the surface of cellulose fibers using commercial cyanide-free electroless copper plating packages commonly available for the manufacturing of printed wiring boards. The deposited copper was found to enhance the thermal stability, electrical conductivity and resistance to moisture uptake of the fibers. On the other hand, the chemistry involved in plating altered the molecular structure of the fibers, as was indicated by the degradation of their mechanical performance (tensile strength and modulus).

Keywords: cellulose; functionalization; copper coating; continuous fibers; electroless plating

1. Introduction

Regenerated cellulose fibers (RCFs) are man-made fibers from naturally occurring cellulose that is spun-formed into continuous, uniform cross-sectional fibers with rather stable physical properties [1]. When compared with natural plant fibers, the properties of RCFs are more application-tunable and less dependent on the cellulose source or the growing–cultivation conditions. Considering their natural origin and

end-of-life disposal, the latest generations of these fibers are more environmentally friendly than the conventional fibers [2,3] used in composites (e.g., glass, carbon) or in textiles (e.g., polyester, polyamide). RCFs are commercially available and are used in various applications with increasing interest in the research and development sectors to improve their performance for use in composites as a reinforcement [4]. In order for these materials to be used in advanced applications, however, not only does their mechanical performance need to be improved, but the addition of new functionalities has also become essential. This can boost their potential limits and suitability for a wider range of applications.

Wearable electronics and electronic casings are examples of applications where electrically conductive functional fabrics are in high demand. The design of conductive cellulose fibers has been approached differently by researchers, for example via the incorporation of graphene during the spinning process of the fiber production [5], or dip-coating the fibers with carbon nanotubes [6]. However, a simpler and more convenient way to achieve conductivity is the use of electroless metal plating on the surface of the fibers. The use of electroless plating to produce conductive cellulose fibers has been reported in the literature, for example in the deposition of a thin layer of copper for microwave applications [7], and in the coating of ferromagnetic material to produce ferromagnetic cellulose microfibers [8] for various electronics applications. Electroless metal coating is very simple and matured process for various applications, such as printed electronics. However, experimental parameters such as the temperature, concentration, and pH of the involved chemistry have a great influence on the properties of the substrate-fibers and the quality of the coating [9]. The reason for this is that the chemical treatment not only modifies the surface but also alters the chemical structure of the cellulose fibers [10]. Recent studies used the approach to produce copper conductive layers on non–conductive lyocell fabrics. This involved preliminary surface activation through silver seeding and bath composition containing HCHO and $C_4H_5KO_6$ at different concentrations [11]. Despite the resulting overall conductive fabric, the risk of losing connectivity at the crossover points between the wrap and the weft is the primary disadvantage of coating fabric rather than individual bundles.

Moreover, the abovementioned and other studies have presented the possibility of coating RCFs with copper to make them conductive, but none of them have addressed the effect of the electroless plating process on their mechanical performance. Thus, this paper studies copper-coated RCFs produced using the electroless process, along with evaluating the effect of different immersion times in a Cu-plating bath on the electrical and mechanical properties of the fibers, including the quality of the coating. The process might be directly incorporated in the production of weaves to make conductive fabric on an industrial scale.

2. Materials and Methods

Bundles of regenerated cellulose fibers (Cordenka 700 Super 3 from Cordenka GmbH, Obernburg, Germany) of 50 mm length were used in this study. The fibers have a semi-circular cross-section of diameter about 12.5 μm. The chemicals used for the electroless plating (perfekto-PEC660) were commercially available solutions from JKEM international, Sweden. Such packages are well known to be optimized for better conductivity, deposited thickness, and adhesion for specific substrate materials.

2.1. Fiber Plating

The process consisted of four main steps in the following sequence: First, the fibers were dipped in a 1:4 Pre DIP Alkaline Catalyst System (ACS) 73 to de-ionized water solution at a pH of 11–12 for 1 minute at 25 °C. Second, they were treated in a bath of 1:4 parts of catalyst ACS 74 to de-ionized water at a pH of 11.5–12.5 for 5 minutes at 40 °C, followed by two washes with de-ionized water for 1 minute per wash. Then, a reducing bath containing 0.5 L reducer ACS 75, 98 L deionized water and a 2 Kg of Boric acid was used at 25–30 °C and a regulated pH of 7 into which the fibers were immersed for 0.5 to 1 minute and washed twice with deionized water for 1 minute each time. In the last step, a copper-plating solution bath was made up with Perfekto Electroless Copper (PEC) 660 components and de-ionized water in the following ratios: 80 de-ionized water, 7.5 PEC 660 A, 5 PEC 660 M, 8 PEC 660 B with the mentioned sequence and accompanied by continuous agitation. The immersion time in the last bath was varied: 15, 30, 45, 60, and 90 minutes.

2.2. Characterization

Microscopy on individual fibers and cross-sections of bundles was performed using a Nikon Eclipse MA200 optical microscope (OM) (Nikon Corporation, Tokyo, Japan) and JEOL JCM-6000 Neoscope scanning electron microscope (SEM) (JEOL technics LTD, Tokyo, Japan). Coated bundles were mounted in an epoxy resin, polished, and their cross-section was investigated. Analysis of the area fraction was performed by separating the components into fractions based on the color contrast. The coating thickness was determined by selecting a coated fiber randomly and averaging the measured thickness at eight radial points. The thickness at the points where the coating was missing was set to zero. The maximum thickness was also based on this random selection and may not represent the actual maximum thickness.

Single fiber tensile tests on 20 mm long fibers were performed to evaluate the mechanical properties. These tests were done on an Instron 4411 universal testing machine equipped with a 5 N load cell and pneumatic grips. Tensile tests were carried out in a displacement-controlled mode with a loading rate of 2 mm/min (corresponding to a strain rate of 10%/min). The strain was calculated from the displacement of the crosshead of the machine taking into account the system compliance with respect to uncoated fibers (UCF). Following the guidelines of the ASTM D3822/D3822M standard, individual fibers, selected randomly from the coated bundles and reference UCF, were carefully separated and glued on paper frames. These frames were cut prior to starting the test. Some fibers broke during mounting on the frames, which may skew the results towards higher strength values. A set of minimum 7 fibers were tested, and the average values are presented.

Fourier-transform infrared (FTIR) (PerkinElmer Inc,Waltham, MA, USA) spectra in attenuated total reflectance (ATR) mode were collected on uncoated and surface copper coated cellulose fibers to detect new absorption bands, if any, during chemical modification. For sample preparation, fibers were cut to be 1 cm long and then analyzed using Perkin Elmer FT-IR Spectrometer. The spectra were recorded after 32 scans with a resolution of 4 cm^{-1} within the range of 4000–700 cm^{-1}.

Thermo-gravimetric analysis (TGA) (Discovery TGA, TA Instruments Inc, New Castel, DE, USA) was used to evaluate the degradation characteristics of the fibers

under a controlled temperature program. Thermo-gravimetric analyzer TGA 5500 was employed to heat from 20–500 °C, at a heating rate of 10 °C/min in nitrogen as carrier gas with flow rate of 30 ml/min.

Electrical resistance measurements of bundles and single fibers were performed at room temperature by 4-wire method using a high precision Fluke 8840A multimeter (Fluke Corporation, Everett, WA, United States). To ease the probing, all measured samples were adjusted to be 50 mm long. Later, measurements were confirmed using the programmable LCR Bridge HM8118 by Hameg instruments (Hameg Instruments, Frankfurt, Germany).

3. Results and Discussion

3.1. Microscopy

Figure 1 shows OM and SEM images of selected samples. Figure 1a of the sample plated for 15 minutes shows that copper was deposited only at some points at the outermost fibers of the bundle. It could also be seen that although the coating on samples with longer immersion times (Figure 1b,c) reproduced the shape of the fiber, the layer of copper was not uniform around the fiber contour. Thus, inhomogeneity could be seen within the coating along an individual fiber as well as in between fibers within the bundle. However, it was concluded that as the immersion time increased, more copper could be successfully deposited on the fiber (see Figure S1 in the supplementary materials for images of the whole bundles). The SEM micrographs show that for a shorter immersion time, the copper particles form a discontinuous layer on the fibers, but due to the inhomogeneity it was not possible to find a representative image for the 15 min or 45 min samples. This is indicated in the supplementary materials (Figure S2). The coating, however, appeared continuous and denser for 60 min and onwards (Figure 1d,e). On the other hand, for the higher deposition time (90 min), the change in thickness and quality of the copper on the fibers was not noticeable, although the number of coated fibers increased.

Systematic measurements of the coating thickness performed on optical micrographs of randomly-selected coated fibers revealed a lower average thickness of the coating

in the 90 min sample (2.72 ± 1.19 μm) than that of the 60 min sample (3.41 ± 1.31 μm), but no significant difference in the maximum measured thickness (7.92 vs. 8.03 μm for 60 min and 90 min, respectively). At the same time, the ratio between the area occupied by the copper and fibers on optical micrographs showed a considerable difference at 90 min when compared to the 60 min immersion time (20% and 8%, respectively). This means that the longer immersion time does not necessarily increase the coating thickness, but it might lead to deeper penetration of copper inside the bundle covering larger surface areas or forming bridges between the coated fibers, bonding them together. This was noticed at several instances during the SEM and OM observations (see the dashed ovals on the OM images of Figure 1). Arrows in Figure 1 point at some areas with imperfect copper/fiber bond. This de-bonding probably occurred during handling of the fibers after coating. This might influence the mechanical properties and the electrical conductivity of the fibers. Further investigations by micro-bond test would help to assess the strength of the fiber–coating and coating–matrix adhesion.

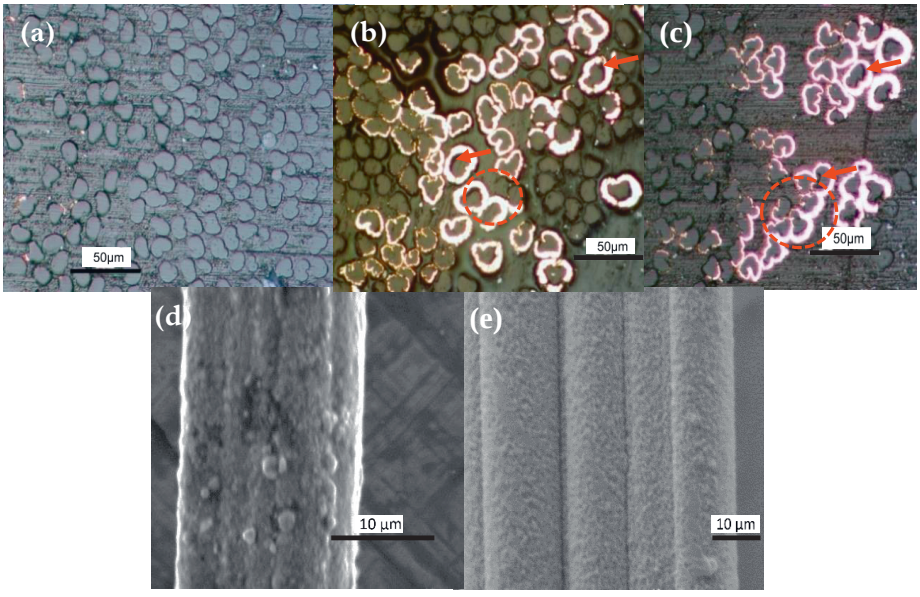

Figure 1. Optical micrographs (OM) of the cross-sections (top) and JEOL JCM-6000 Neoscope scanning electron microscope (SEM) images of the fiber surface (bottom) of (**a**) coated fibers after 15 min, (**b,d**) 60 min, and (**c,e**) 90 min immersion time in a Cu-plating bath.

3.2. Electrical Properties

Measurement of the electrical resistance on bundles rather than on individual fibers is more practical and relevant to the application of fibers in composites, since the final product (textiles and composites) would be made of bundles rather than single filaments. This is also evident from the graphs in Figure 2, since the resistance of the bundles compared to single filaments was always lower for the same immersion time. According to the experiments, the immersion time of 15 minutes only led to measured resistance in the MΩ ranges, thus the bundles practically remained non-conductive. In such cases, samples have always resulted in matt surfaces as shown in Figure S3. However, the conductivity continued to increase by increasing the immersion time. This supports the claim of having new contact points from the larger surface area of the deposited copper, which is likely to penetrate deeper into the bundle.

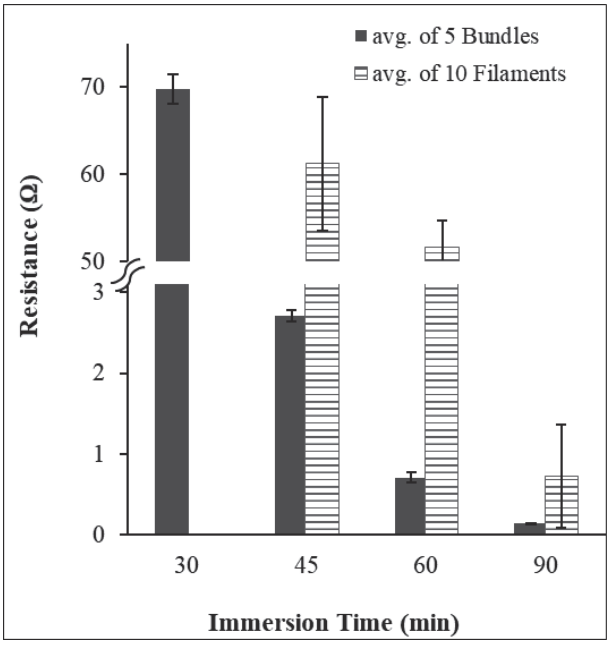

Figure 2. Electrical resistance of 50 mm long samples.

3.3. Mechanical Properties

Due to the limited amount of sample, and seeking a proof of concept, the mechanical properties were investigated on individual fibers rather than on bundles. Figure 3 shows the mechanical properties of the UCF and coated fibers for different Cu-plating times. The tensile properties of the fibers have been largely degraded. Stiffness and strength of the single fibers for the 15 min immersion time decreased by around 10% and 70% respectively when compared with UCF. It is possible that exposing the fibers to chemicals in the plating process causes relaxation of the molecules leading to a loss of orientation and disorder in the fiber microstructure [12]. The orientation of the cellulose chains is responsible for its mechanical performance and is attained during the manufacturing process by stretching the fibers along the axial direction. It is reasonable then, to consider that if these chains are allowed to relax by any external factor, they tend to form a more amorphous structure and lose their orientation, leading to reduced mechanical performance. Copper, on the other hand, is a rigid metal compared to the soft fibers (the stiffness of copper is estimated around 128 GPa [13]) and its presence on the surface of the fibers is responsible for increasing their stiffness and compensate for the stiffness lost during the chemical treatment. However, due to its brittleness it does not contribute to the strength. This was further investigated by FTIR analysis. However, no significant difference is noticed in the strength of the samples at different immersion times, indicating that the degradation occurred either during the fiber-surface-activation process or immediately after immersion in the copper-plating bath. To confirm this statement, additional investigation should be carried out. After 90 min immersion time, the fibers seem to retain some of their properties, since the stiffness loss was only 8%. As mentioned above, this is possibly due to the support provided by the large amount of copper deposited on the fibers.

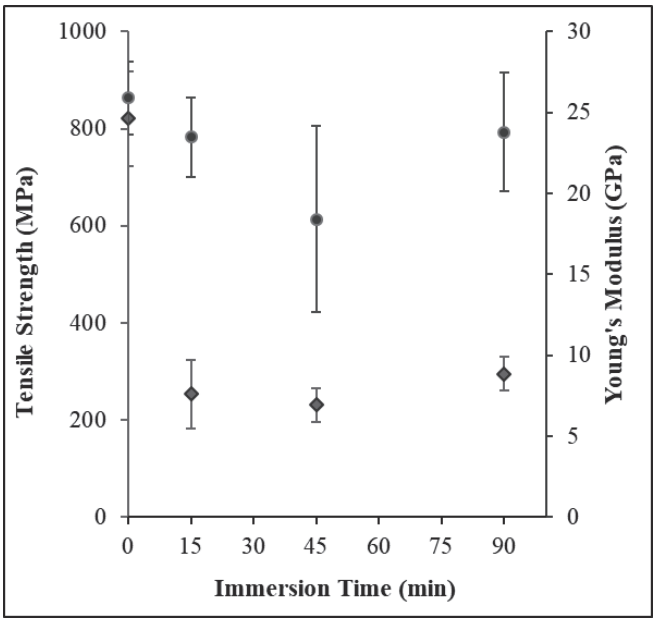

Figure 3. Mechanical properties: (circles: modulus, rhombus: strength).

3.4. Spectral and Gravimetric Analysis

FTIR-ATR spectroscopy, which is a surface-sensitive technique, can illustrate changes in the spectra after chemical treatments. Figure 4A shows the spectra of UCF and copper-coated fibers at 15 min, 45 min, and 90 min immersion time. Compared to UCF (spectrum "a"), the spectra of coated fibers presented changes, particularly peaks between 1200 and 800 cm^{-1}, and bands between 3000 and 2800 cm^{-1}, indicated by arrows. For the 15 and 45 min immersion times, a peak appeared around 1060 cm^{-1} which can probably be ascribed to the vibration of the Sn–OH bond [14]. This peak disappeared for the 90 min immersion time, which indicates that no more free Sn–Pd molecules were present over the surface of the fiber, and copper is present at all the activated sites. The spectra of the coated fibers showed an extra peak at 2938 cm^{-1} that corresponded to C–H asymmetric stretching in a new molecular environment.

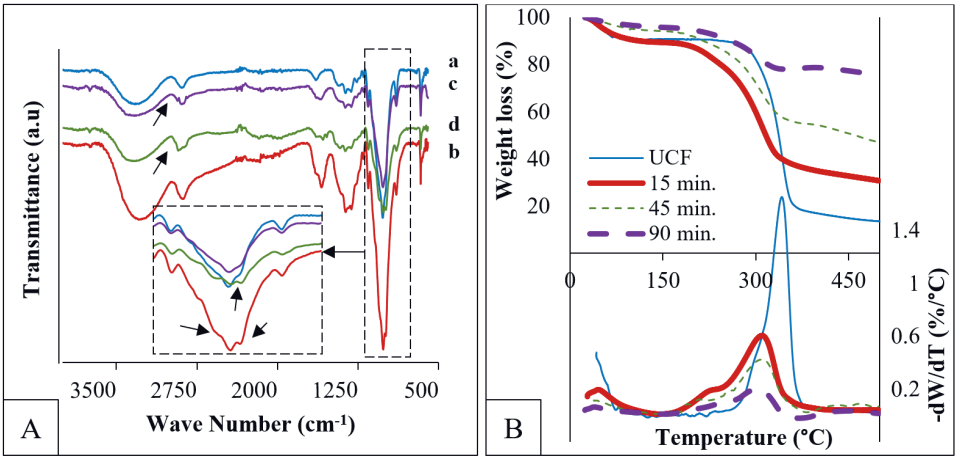

Figure 4. (**A**) Fourier-transform infrared (FTIR) analysis: a, b, c, d spectra correspond to uncoated and coated fibers for 15 min, 45 min, and 90 min respectively; (**B**) Thermo-gravimetric analysis (TGA) (top) and derivative of thermo-gravimetric curves (bottom).

Figure 4B shows the thermal behavior of the fibers by TGA before and after coating at three different immersion times. The mass loss curves showed three different stages for all fibers. The initial stage extending up to 100 °C is attributed to the evaporation of the adsorbed water on fibers and already shows the difference in their moisture uptake. It can be observed that the sensitivity of fibers to moisture was reduced with the increased concentration of copper.

The second stage largely differed between fibers, corresponding to the degradation of cellulose. The degradation of UCF occurred in a very short range of temperatures between 280 °C and 360 °C [15], leading to more than 70 wt% loss. However, the degradation of all copper-coated fibers started at the same temperature of ~180 °C and spread over an extended range of temperatures, ending at 360 °C (same endpoint as UCF). This is indicated by the difference in the peak size in the derivative of the TG curves. The peak for UCF was higher (indicating greater weight loss) and narrower (indicating the shorter interval over which the weight loss occurs), while all other peaks for the coated fibers were broadened and had a smaller amplitude. The weight loss intensity drop can be attributed to the decrease in the relative amount of cellulose (an increase in the amount of copper), while the shift in the degradation

temperature might be attributed to the chemical degradation of cellulose chains during the electroless plating process. The polymeric chains became shorter due to the effect of the chemicals and hence was more susceptible to the subsequent thermal degradation.

The weight loss of the coated fibers showed a difference according to the immersion time, with 51 wt%, 37.5 wt%, and 17 wt% loss for 15, 45, and 90 minutes, respectively. As the immersion time increased, the degradation temperature was not strongly affected, which may be an indication that the immersion time in the copper-plating bath had no significant effect on the degradation. The final region extending to 500 °C corresponded to the ash contents (residual weight) obtained at the end of the TGA measurement.

4. Conclusions

The possibility of coating commercially-available continuous cellulose fibers with a commercial cyanide-free electroless copper deposition solution to achieve electrically conductive cellulose fibers was investigated. Preliminary results showed the increase in conductivity by increasing the immersion time in the copper-plating bath, trading-off with the loss in mechanical performance due to the sensitivity of these fibers to the chemicals. From the results, it can be concluded that the conditions of the copper-coating process should be optimized to minimize damage. On the other hand, longer times in the copper-plating bath helped to achieve a more uniform coating until 60 min, which might be considered the optimal coating time.

Supplementary Materials: The following are available online at http://www.mdpi.com/2079-6439/7/5/38/s1, **Figure S1:** The top image is the full bundle, coated for 60 min, embedded in epoxy resin. The bottom images are images forming the whole of the bundle for the 90 min spread and embedded in matrix of epoxy. **Figure S2:** SEM images for the 45 min coating time. The images show that in some parts of the fiber, the coating was discontinuous, but in other parts it was continuous, which makes it difficult to assess the quality of the coating after this

plating time. **Figure S3:** Micrographs of bundles showing the change in color after immersion in a copper-plating bath for 15 min (left) and 90 min (right).

Author Contributions: conceptualization, A.H. and A.R.; methodology, A.H., A.R., Z.A.-M., R.J.; formal analysis and investigation, Z.A.-M., A.H., A.R., A.O., S.S.C., R.J.; data curation, Z.A.-M; writing—original draft preparation, Z.A.-M and A.H.; writing—review and editing, Z.A.-M., A.H., A.R., A.O., S.S.C., R.J.; visualization, Z.A.-M., A.H. and R.J. ; supervision, R.J.; project administration, A.H. and R.J.; funding acquisition, A.H. and R.J.

Funding: This research was funded by the Swedish Foundation for International Cooperation in Research and Higher Education, STINT, grant number IB2017-7389. The APC was funded by Luleå University of Technology.

Acknowledgments: The authors would like to acknowledge the support from the Smart-WPC project within the framework of Interreg-Nord projects.

Conflicts of Interest: The authors declare no conflict of interest. The funders had no role in the design of the study; in the collection, analyses, or interpretation of data; in the writing of the manuscript, or in the decision to publish the results.

References

[1] Santamala, H.; Livingston, R.; Sixta, H.; Hummel, M.; Skrifvars, M.; Saarela, O. Advantages of regenerated cellulose fibres as compared to flax fibres in the processability and mechanical performance of thermoset composites. Compos. Part A 2016, 84, 377–385.

[2] Shen, L.; Patel, M.K. Life cycle assessment of man-made cellulose fibres. Lenzinger Berichte. 2010, 88, 1–59.

[3] Yu, M.C.; Wan, J.X. Environmental Friendly Development of Regenerated Cellulose Fiber Production. DEStech Transactions on Engineering and Technology Research, 2017. Available online: URL http://www.dpi-proceedings.com/index.php/dtetr/article/view/11079 (accessed on 26 April 2019).

[4] Das, M. Man-made cellulose fibre reinforcements (MMCFR). In Biocomposites for High-Performance Applications, Ray, D., Ed.; Woodhead Publishing: Cambridge, UK, 2017; https://doi.org/10.1016/B978-0-08-100793-8.00002-8, pp. 23–55.

[5] Mahmoudian, S.; Reza Sazegar, M.; Afshari, N.; Uzir Wahit, M. Graphene

reinforced regenerated cellulose nanocomposite fibers prepared by lyocell process. Polym. Compos. 2017, 38, 81–88.

[6] Qi, H.; Liu, J.; Mäder, E. Smart cellulose fibers coated with carbon nanotube networks. Fibers 2014, 2, 295–307.

[7] Zabetakis, D.; Dinderman, M.; Schoen, P. Metal-Coated Cellulose Fibers for Use in Composites Applicable to Microwave Technology. Adv. Mater. 2005, 17, 734–738.

[8] Dinderman, M.A.; Dressick, W.J.; Kostelansky, C.N.; Price, R.R.; Qadri, S.B.; Schoen, P.E. Electroless plating of iron onto cellulose fibers. Chem. Mater. 2006, 18, 4361–4368.

[9] Sittisart, P.; Hyland, M.M.; Hodgson, M.A.; Nguyen, C.; Fernyhough, A. Preparation and characterization of electroless nickel-coated cellulose fibres. Wood Sci. Technol. 2014, 48, 841–853.

[10] Shchipunov, Y.; Postnova, I. Cellulose Mineralization as a Route for Novel Functional Materials. Adv. Funct. Mater. 2018, 28, 1705042.

[11] Root, W.; Aguiló-Aguayo, N.; Pham, T.; Bechtold, T. Conductive layers through electroless deposition of copper on woven cellulose lyocell fabrics. Surf. Coatings Technol. 2018, 348, 13–21.

[12] Hajlane, A.; Kaddami, H.; Joffe, R.; Wallström, L. Design and characterization of cellulose fibers with hierarchical structure for polymer reinforcement. Cellulose 2013, 20, 2765–2778.

[13] Dolbow, J.; Gosz, M. Effect of out-of-plane properties of a polyimide film on the stress fields in microelectronic structures. Mech. Mater. 1996, 23, 311–321.

[14] Joy, M.; Nair, B.N.; Mohamed, A.A.P.; Warrier, K.G.; Hareesh, U.N.S. One-Pot Hydrothermal Synthesis of Visible-Light-Responsive MoS2/g-CNO Heterostructures for Organic-Pollutant Degradation. Eur. J. Inorg. Chem. 2016, 24, 3912–3920.

[15] Carrillo, F.; Colom, X.; Sunol, J.J.; Saurina, J. Structural FTIR analysis and thermal characterisation of lyocell and viscose-type fibres. Eur. Polym. J. 2004, 40, 2229–2234.

Conductive Regenerated Cellulose Fibers (RCFs) by Electroless Plating

Zainab Al-Maqdasi[1], Abdelghani Hajlane[2], Abdelghani Renbi[1], Ayoub Ouarga[2], Shailesh Singh Chouhan[1] and Roberts Joffe[1]

[1] Luleå University of Technology, Luleå, 97187, Sweden
[2] Mohammed VI Polytechnic University, Benguerir, 43150, Morocco

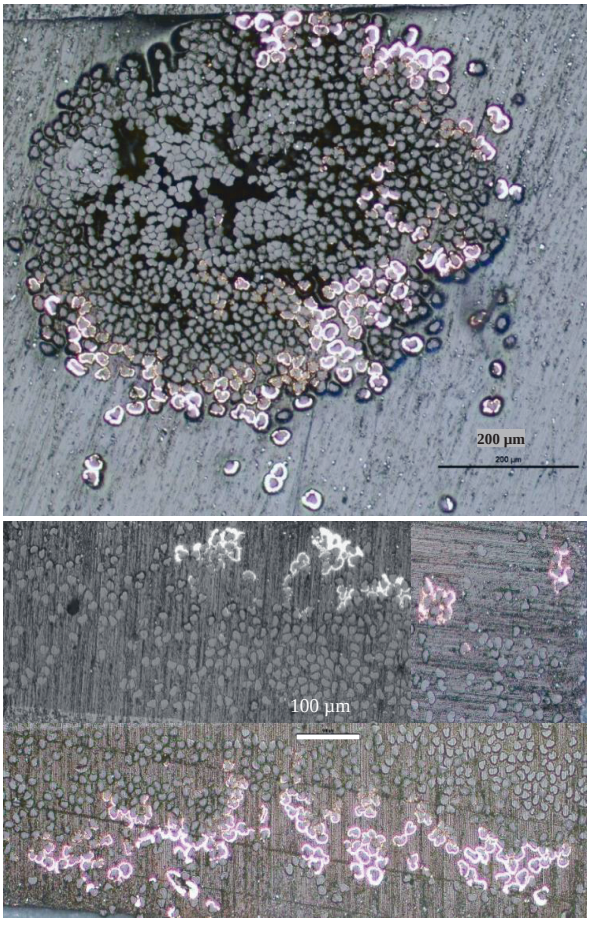

Figure S1. The top image is for the full bundle of 60 min coating time, embedded in epoxy matrix. The bottom is stitched images forming the whole of the bundle for the 90 min, spread and embedded in a matrix of epoxy.

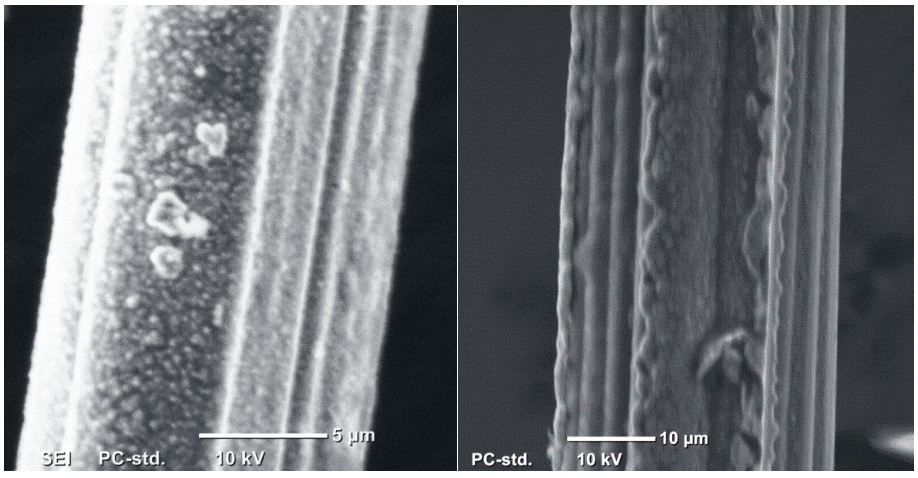

Figure S2. SEM images for the 45 min coating time. The images show that in some parts of the fiber, the coating was discontinuous but in other parts it was continuous, which makes it difficult to assess the quality of the coating.

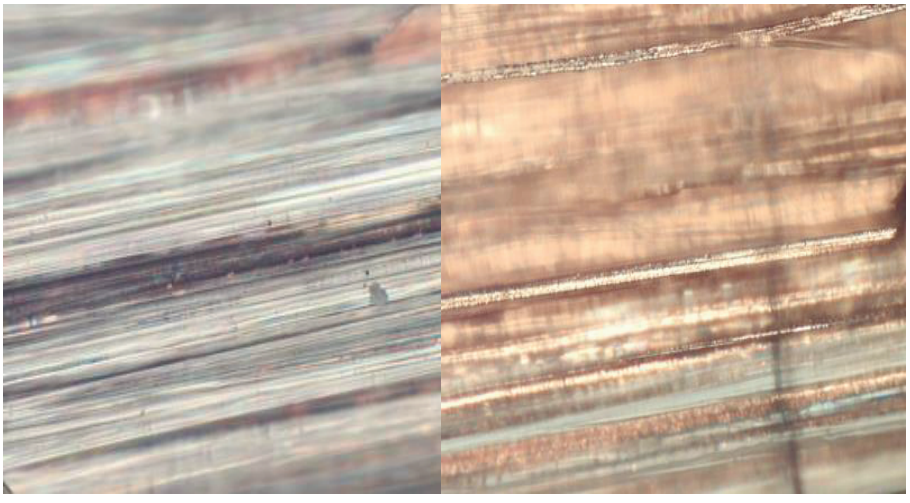

Figure S3. Micrographs of bundles showing the change in color after immersion in Cu-plating bath for 15 min (left) and 90 min (right).

Paper II

Characterization of Wood and Graphene Nanoplatelets (GNPs) Reinforced Polymer Composites

Zainab Al-Maqdasi, Guan Gong, Birgitha Nyström, Nazanin Emami, Roberts Joffe

Original Research Paper

Characterization of Wood and Graphene Nanoplatelets (GNPs) Reinforced Polymer Composites

Zainab Al-Maqdasi[1], Guan Gong[2], Birgitha Nyström[2], Nazanin Emami[1], and Roberts Joffe[1]

[1]Luleå University of Technology, SE 971 87, Luleå, Sweden
[2]RISE SICOMP AB, SE 941 26, Piteå, Sweden

Abstract

The paper investigates the utilization of commercial masterbatches of graphene nanoplatelets and available conventional manufacturing techniques to improve properties of polymers and composites. The effect of aspect ratio of the graphene platelets (represented by the different number of layers) on the properties of high-density polyethylene is investigated. Produced composites were characterized for their mechanical properties (tensile, flexural, impact) and physical characteristics (moisture uptake, thermal stability). Effect of the addition of the nanoplatelets on the thermal conductivity and diffusivity at different filler content was also investigated. In general, the mechanical performance of the composites was enhanced at the presence of either of the reinforcements. The improvement in mechanical properties of the nanocomposite was notable considering that no compatibilizer was used in their manufacturing. This can help development of composites on an industrial scale without modification of the currently used manufacturing techniques.

Keywords: Graphene Nano-platelets (GNPs), masterbatch, nanocomposite, wood polymer composites (WPC), energy transport, high density polyethylene (HDPE)

1. Introduction

The growing awareness of environment and the demands for increasing the sustainability in resources and industries have urged the development of bio-based materials for use beyond their structural applications. Production of bio-based materials such as wood polymer composites (WPCs) with added functionalities such as thermal or electrical conductivities can partially answer for these demands. This can be made possible by profiting from the advances in the research and technology of nanomaterials.

Since the discovery of graphene, it has been largely researched being termed the material of the future due to its remarkable properties. Graphene is a 2D carbon allotrope material (thickness of one carbon atom) with strength and stiffness of 100 GPa and 1 TPa, respectively. Thermal and electrical conductivities of graphene are estimated to be 5000 W/m K and 6000 S/cm [1]. This is higher than conductivities of some metals such as copper, for which thermal conductivity is known to be ~400 W/m K. These properties which are result of the unique structure and bonding nature of the atoms in the lattice, together with high aspect ratio make graphene an ideal reinforcing material to the polymers to produce high performing composites. When embedded in the matrix, these nano-modifiers can contribute to the enhancement of the conductivities of the host material resulting in added functionality. The application of graphene nanoplatelet (GNPs) in composites is foreseen to grow between 2018-2025 to about 40% in terms of revenue-based compound annual growth rate (CAGR) as it is being increasingly used in composite-utilizing industries such as construction, aerospace and the automotive [2,3].

Incorporation of different graphene-based derivatives has shown positive effect on the thermal, electrical or mechanical properties for variety of thermoplastics such as PLA [4], PVA [5], PET [6,7], PA [8]. For example, the mechanical properties of high-density polyethylene (HDPE) were continuously enhanced with the addition of GNPs up to 15 wt% [9]. Moreover, 16% improvement in thermal conductivity of HDPE nanocomposites prepared by melt-mixing process was achieved at a graphene content of only 1 wt% [10]. Similarly, these particles were found to improve the

properties of wood polymer composites (WPC) [11,12]. However, in the case of WPC, a compatibilizer is usually employed to increase the adhesion between the wood filler to the polymer which has also been reported to increase the compatibility of the GNPs with the polymer matrix [13].

One of the main challenges of reinforcing polymers with graphene is its tendency to aggregate and restack which results in a reduced graphene/polymer contact area and limited load transfer efficiency. Selection of production method of the nanocomposite [14] and chemical functionalization of graphene [4] have been found to play a role in reducing the impact of the abovementioned problem. Solution mixing and in-situ polymerization of the polymers in the presence of these particles are found to be efficient processes to produce well-dispersed nano-particles in the polymers [15]. Nonetheless, among other disadvantages, these processes are not easily scaled up and difficult to provide the large amounts required in industrial production. On the other hand, the melt mixing is more cost-effective method that utilizes the conventional processing techniques of polymers such as screw extrusion. In some cases, this technique would still require dealing with and handling the dry form of the nanoparticles which can be hazardous and challenging to feed to the equipment due to their low bulk density [16].

Functional compatibilization of graphene by covalent and noncovalent bonds would lead to better dispersion in the polymer either as a result of the bulky groups attached to the surface or by the strong polar interactions [17]. The covalent functionalization can result in reduced electron-transport ability when the ratio of O/C increases [18,19] while the noncovalent bond can improve the conductivity due to the improved compatibility with the polymer matrix [20]. Therefore, these two factors should be considered when balancing between graphene dispersion state and composite conductivity.

Recently, tackling these problems have been made easier with the emerging technology of the patented masterbatches [21]. Such materials are polymers with high content of the nanoparticles (graphene, carbon nanotubes or clay platelets) which are well dispersed using scalable, environmentally friendly techniques [22] and ready to

be mixed with base polymer to prepare the composite by melt mixing. This technique ensures easy dispersion and high throughput of materials while at the same time achieving improved mechanical and functional properties. Several commercial masterbatches are available based on different polymers and polymer grades.

In this work, commercial masterbatch of graphene nanoplatelets (GNPs) in high density polyethylene (HDPE) was used to enhance the physico-mechanical properties of the polymer. These platelets are functionalized at the edges which ensures improved compatibility with the polymer while preserving the characteristics of graphene in the bulk. Nanocomposites were manufactured without the addition of a coupling agent and in a single run through the extruder. The synergistic effect of reinforcing the polymer with wood and GNP in the presence of limited amount of coupling agent is also investigated. The choice of material and the production technique contribute to the development of sustainable industry and products without the need for sophisticated processes.

2. Experimental

2.1. Materials

Thermoplastic of High-Density Polyethylene (HDPE) (MG9647S) in the form of pellets was purchased from BOREALIS AG (Vienna, Austria). Two HDPE-based masterbatches with edgily-functionalized carbon platelets additives from NanoXPLOre (Montreal, Canada) were used. The first is heXo HDPE1-V20/35 (further denoted as M1) with 35 wt% dispersed Graphene Nanoplatelets (GNPs) having average thickness of 20 nm, flake size of 50 μm and the number of layers in one platelet is ~40. The second contains 25 wt% Graphene Black™ 3X (further referred to as M2) having 6-10 layers and a particle size of 38 μm. According to the manufacturer, the functionalization of the platelets resulted in an oxygen content that did not exceed 7 wt% in both masterbatches. The wood flour (WF) is sawdust of spruce and pine wood with 75% of its particles in the size range 200- 400 μm. Maleic anhydride-grafted high-density polyethylene (MAPE), E265, kindly provided by DuPont, was used as compatibilizer in WPC.

2.2. Fabrication of the composites

Selected content of GNPs in the nanocomposites were manufactured by feeding the masterbatch with neat polymer into a co-rotating twin screw extruder ZSK25 (Krupp Wener & Pfleiderer GmbH, Germany). The operation parameters and temperatures of the extruder are presented in Table 1 while sample nomenclature with its composition is presented in Table 2. With the same parameters, WPC and the GNP-modified WPCs were prepared. The wood flour was dried overnight in the oven at 100°C then fed through the side feeder into extruder while all other components (HDPE, MAPE and masterbatch) were mixed and fed through the main feeder. All wood composites (with and without GNPs) were run through the extruder twice with the parameters of "Round 1" and "Round 2" from the table while the nanocomposites went a single run (only "Round 2" in the table).

Measured amounts of the extrudate were heated in an infrared oven for 30 min at 220°C then compression molded using a conventional 310-ton compression molding press (Fjellman, Sweden). The resulted rounded plates having the dimensions of 320 mm in diameter and 4 mm in thickness which were then cut to samples dimensions using waterjet. For the neat polymer, pellets were directly melted, and compression molded in the same conditions except that they were not extruded.

Table 1. Parameters of the extrusion process.

	Parameter (unit)	Value
Round 1	Temperature range (°C)	180-200
	Mass flow (kg/h)	10
	Rotation speed of head screw (rpm)	300
Round 2	Mass flow (kg/h)	8
	Rotation speed of head screw (rpm)	120

Table 2. Name and composition of the investigated samples.

Sample code	HDPE (wt%)	GP (wt%)	WF (wt%)	MAPE (wt%)
PE	100	-	-	-
PE2-M1	98	2	-	-
PE2-M2				
PE6-M1	94	6	-	-
PE15-M1	85	15	-	-
PE15-M2				
25WPC	74	-	25	1
40WPC	58.5	-	40	1.5
25WPC10	63.9	9.6	25	1.5
40WPC7.5	50.9	7.6	40	1.5
40WPC15	43.5	15	40	1.5

2.3. Characterization

Tensile test: Samples with dimensions of 15 mm by 200 mm (100 mm gauge length) were tested on Instron 3366 universal testing machine equipped with 10 kN loadcell and pneumatic grips in an extension control mode with a cross head speed of 5 mm/min for the neat polymer and nanocomposite and 2 mm/min for the WPCs (since the gauge length was 100 mm these loading rates correspond to strain rates of 5 %/min and 2 %/min respectively). Strain was measured by extensometer with base length of 50 mm. An initial loading-unloading step with maximum applied strain up to 0.2% was performed to measure initial stiffness of undamaged material. Assuming linearity of behavior in this region, stiffness was obtained from the slop of the unloading segment between 0.2%-0.05% strain. Later, the sample was loaded with the same rate until limitation of the extensometer was reached. The yield stress was obtained at the intersection point of the stress- strain curve with the 0.2% offset strain line following guidelines of the ASTM D638. A minimum of 5 valid tests were conducted and the results are the average of recorded values.

Impact test: Impact strength was determined by performing impact test on Charpy set up (WPM Leipzig, Germany). This machine is equipped with a hammer capable

of providing a maximum breaking energy of 14.7 J for a sample resting on supports separated apart by 30 mm with an impact velocity of 3.8 m/s. The equipment was calibrated according to the ASTM standards D6110-10 and the energy value readings were corrected to the windage of the hammer and the energy losses due to the friction. Specimens (5 per test) of dimensions of 125 mm by 12.7 mm were notched manually with a razor blade to the possible accuracy on one edge and impacted on the opposite unnotched edge. The accuracy of the notch was not taken as assessment criteria for the validity of the specimen for test. The reported impact strength is the result of dividing the net breaking energy by the total area of the developed crack (cross section area of the unnotched portion of the specimen).

Moisture uptake: Three specimens of each sample material with dimensions of 16 mm by 80 mm were used for the determination of moisture uptake behavior. Prior to the test samples were dried in the oven at 40°C until the difference between two successive measurements was negligible then edge-sealed with water repellent commercial Silyl-modified polyether (Casco, Sweden) to insure one dimensional moisture uptake. Samples were weighed and placed in a plastic container with water at 40 °C (specimens were not immersed but suspended over the water with measured relative humidity RH=99%). Moisture uptake was monitored by frequent measurements of sample weight on AG245 precision scale (from METTLER Toledo). Moisture dimensional stability was assessed by thickness measurements before and after exposure to moisture. These samples were later tested for flexural properties for comparison with non-conditioned samples. It is worth noting that during weighing or testing the relative humidity in the lab was different than the conditioning environment which might have caused uncontrolled diffusion of moisture into or from the specimen. However, care was taken to minimize the exposure of samples to these conditions.

Flexural test: Following guidelines of ASTM D790, flexural properties were determined by means of three-point bending test setup on an Instron 4411 machine equipped with 5 kN load cell. Five specimens having dimensions 80 mm, 16 mm and 4 mm (length, width and thickness) with a support span distance to thickness ratio of 16:1 were tested with a cross head speed assuring straining the outer fibers by

a rate similar to that of the tensile test (2 %/min and 5 %/min for the nanocomposites and WPCs respectively).

Crystallinity and thermal properties: Differential Scanning Calorimetry (DSC) was used to determine the degree of crystallinity in the polymer as well as the characteristic temperatures. Samples of weight 5-10 mg, encapsulated in aluminum pans with pierced lids, were subjected to a thermal profile in nitrogen atmosphere (gas flow of 80 ml/min). Temperature was raised from 25°C to 200°C (past the theoretical melting point of HDPE) in a rate of 10 °C/min and kept under isothermal conditions (200 °C) for 5 minutes to erase thermal history, then cooled to room temperature with a rate of 20 °C/min using liquid nitrogen. Melting onset and peak value as well as crystallization temperatures were determined from the endothermic and exothermic peaks of the DSC curve, respectively. Crystallinity was calculated from the heat of fusion obtained by integrating the endothermic peak between 60°C and 180°C according to the following formula:

$$\%X_c = \frac{\Delta H_f}{\Delta H_f^0} \times \frac{1}{1 - W_f} \times 100 \quad (1)$$

where ΔH_f is the heat of fusion of the sample, ΔH_f^0 is the heat of fusion of 100% crystalline PE and was taken to be 293 J/g [23], and W_f is the weight fraction of the fillers.

Hot disc thermal constants analyzer TPS 500 was used to determine the thermal conductivity and thermal diffusivity of the material. Squared 40 mm × 40 mm samples with a nominal thickness of 4 mm were tested at room temperature using the room temperature sample holder. Based on the available probing depth, the sensor 5465 was selected that have a radius of 3.186 mm and enclosed in Kapton insulation films. Measurement time was 2.5 s with a heating power of 96 mW assuming isotropic material. The experiment was performed in a series of 5 measurements per sample with a waiting time of 15 minutes between the measurements. Values presented are the average of these five measurements. It is

worth noting, though, that the total to characteristic time was not the optimum due to the limited available sample size.

Thermal mechanical analyzer (TMA/SDTA841^e from METTLER TOLEDO) was used to investigate directionality in thermal dimensional stability of the samples in oxygen environment and following a predefined thermal profile. Samples were subjected to two cycles of thermal profile where they were heated to 110°C in a rate of 2 °C/min and brought back to room temperature (23°C). A very small load of 0.02 N as applied on the sample to minimize disturbance. Samples of the same material were tested in two different directions, one parallel to the direction of compression molding and the other is perpendicular to it.

Morphology: The composites were characterized by scanning electron microscopy (JEOL JCM-6000 Neoscope) on test-fractured surfaces or freeze-fractured surfaces sputter-coated with thin layer (<15 nm) of conductive element (gold or palladium) while the distribution and state of dispersion of the particles was qualitatively assessed by computer tomography using 3D X-ray micro-tomography (Zeiss Xradia 510 Versa). It is important to define a coordinate system in order to understand the viewing plane for the samples when referred to later in the discussion. These are found in Figure 1 where the solid-painted face (x-y plane) represents the compression molding face.

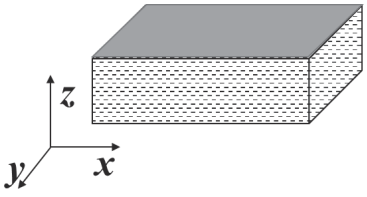

Figure 1. Defined coordinate system with respect to compression molding surface.

3. Results and Discussion

3.1. Tensile Properties

Representative stress-strain curves of the polymer and composites are plotted in Figure 2. Despite the obvious change of response towards stiffer and stronger material for the nanocomposite compared to the neat polymer, samples did not break during the test even after exceeding 8% strains. For the sake of fair comparison, the curves are presented until 6% for all samples. There is a gradual increase in stiffness with the increase in graphene content which is also shown in numerical values tabulated in Table 3. It is also noticeable that masterbatch M2 is more effective in reinforcing the composite than M1 that have higher number of graphene layers in the platelet. Improvement by addition of 2 wt% GNP of masterbatch M2 in polymer competes or even exceeds material with 6 wt% GNP of M1 in some cases. For the same content of GNPs in polymer, there is always higher improvement of properties for the M2 system over that of M1. This is due to the fewer number of graphene layers in M2 that results in increased aspect ratio of the platelets and larger graphene-polymer contact surface area. With properties of neat polymer being the reference values, a maximum improvement of 140% and 79% was achieved for the tensile stiffness and stress at yield respectively for sample PE15-M2 and a minimum of 12% and 2% (modulus and yield stress) after the addition of 2 wt% GNP (PE2-M1).

Similarly, WPC witnessed improved tensile properties with the addition of GNPs. These are presented in the stress-strain curves (Figure 2b) as well as in Table 3. In this case, though, the composite became too brittle and the elongation at break was reduced to below 4% and just above 1% at the presence of 15 wt% GNP in 40 wt% wood composites. Regarding the WPC it is possible to separate the effect of WF from that of the GNPs. The improvement in the 40WPC15 sample in terms of the stiffness and stress at yield is 219% and 146% if compared to the neat polymer while the same parameters were improved by 50% and 14% with respect to the WPC (base value for 40WPC).

In a previous study [24], the improvement in stiffness of HDPE reinforced with similar amount of GNPs used in this study was inferior to the values reported here

considering the lower properties of the starting materials and the use of large amounts of compatibilizer that suggest higher expectations for improvement upon the addition of the reinforcement. Furthermore, skipping the necessity to deal with the nano-particles in their hazardous dry form works for the favor of using the masterbatch despite the similarity of the used processing method.

Earlier research [11,12] reported a decrease in the properties of the WPC after a certain additive content (typically below 5 wt%) and attributed that to the possible agglomeration of these particles that act negatively on the mechanical performance of the composite. However, it does not seem to be the case here and the improvement is confirmed until up to 15 wt% content of nano-reinforcement.

Table 3. Tensile properties of the nanocomposites and WPCs.

Sample	E [std] (GPa)	σ_{max} [std] (MPa)	σ_{Yield} [std] (MPa)	ϵ_{Yield} [std] (%)
PE0	1.89 [0.06]	22.47 [0.57]	8.40 [0.34]	0.65 [0.03]
PE2-M1	2.11 [0.11]	22.71 [0.35]	8.54 [0.15]	0.60 [0.02]
PE2-M2	2.42 [0.13]	25.61 [0.28]	9.94 [0.12]	0.61 [0.02]
PE6-M1	0.49 [0.05]	23.46 [0.32]	9.90 [0.96]	0.58 [0.01]
PE15-M1	3.85 [0.19]	26.40 [0.53]	12.84 [0.45]	0.54 [0.01]
PE15-M2	4.54 [0.35]	29.33 [1.15]	15.05 [0.93]	0.53 [0.01]
25WPC	2.88 [0.33]	26.56 [0.75]	13.60 [0.68]	0.67 [0.07]
25WPC10	4.48 [0.25]	27.66 [0.46]	16.67 [0.46]	0.57 [0.02]
40WPC	4.01 [0.23]	32.34 [1.17]	18.12 [1.50]	0.65 [0.03]
40WPC7.5	4.77 [0.27]	29.98 [1.16]	18.88 [0.85]	0.60 [0.01]
40WPC15	6.03 [0.17]	28.33 [0.94]	20.69 [0.80]	0.54 [0.01]

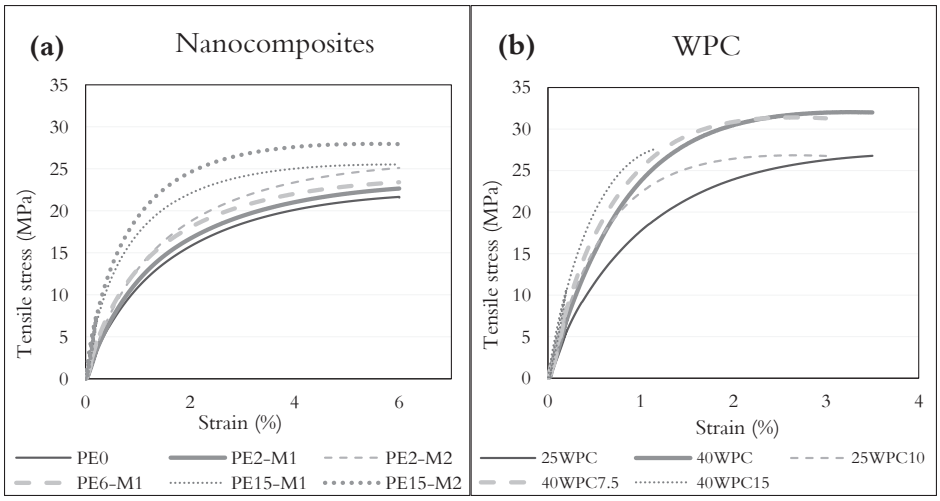

Figure 2. Tensile stress-strain curves of the nanocomposites (a); and wood polymer composites (b).

3.2. Impact Strength

The impact strength of the nanocomposites and the WPCs are shown in Figure 3. The addition of the nanoplatelets has a positive effect on the impact strength of the polymer. The rigid particles may induce new forms of energy dissipation that leads to delayed fracture. These can be in form of pull outs, crack pinning [25] or bridging the polymer chains and redirecting the crack to new paths before the final fracture. Layer sliding is another form of toughening associated with the layered reinforcement [26], due to the consumed energy in overcoming the forces binding the layers in the platelet. However, at higher loadings, where agglomerations are expected, the pull-out of big agglomerates is easier and requires less energy and thus the resistance to crack propagation is reduced. It is also possible that these agglomerates act as new sites for crack initiation that enhance energy dissipation and thus, competing mechanisms of toughening occur. The addition of wood results in marginal or negative effects on the impact strength of the polymer which is only compensated at high GNPs loadings.

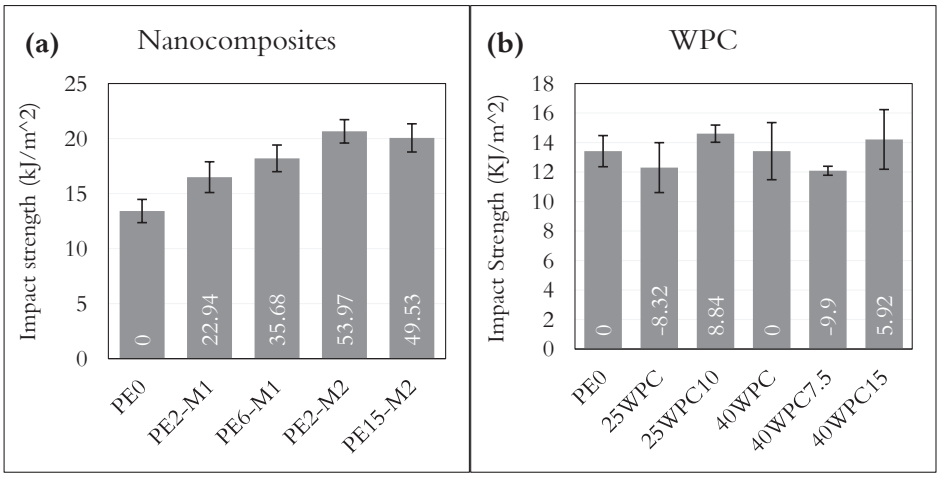

Figure 3. Impact strength of the nanocomposites (a); and the wood polymer composite (b) at different graphene and wood fiber contents. Data label is the % change with respect to neat polymer.

3.3. Morphology

Freeze- fractured surfaces (broken after immersion in liquid nitrogen) of the samples under SEM are shown in Figure 4. The morphology of the sample is changing from topological surface, with fibrils-forming fracture for neat polymer (Figure 4a), to a more smoothened surface and brittle-like fracture for the GNP-reinforced materials (Figure 4b). From the figure, it could also be seen that particles are well distributed in the polymer as they span the image evenly. This even distribution supports the consistent improvement achieved in the tensile properties of the reinforced polymer. The large folded particle is also seen in the image which might act as defected area for a premature failure due to the week bonding with the polymer. The void surrounds it can be a pocket for water as well. However, despite the good distribution, observing Figure 4c, gives an evidence that the dispersion state can still be improved. The image shows a particle with thickness about the size of the scale bar which is much higher than the thickness provided by the supplier, indicating that this particle is a restack of multiple platelets. This would also mean that there is a greater potential and margin of improvement if better dispersion can be achieved.

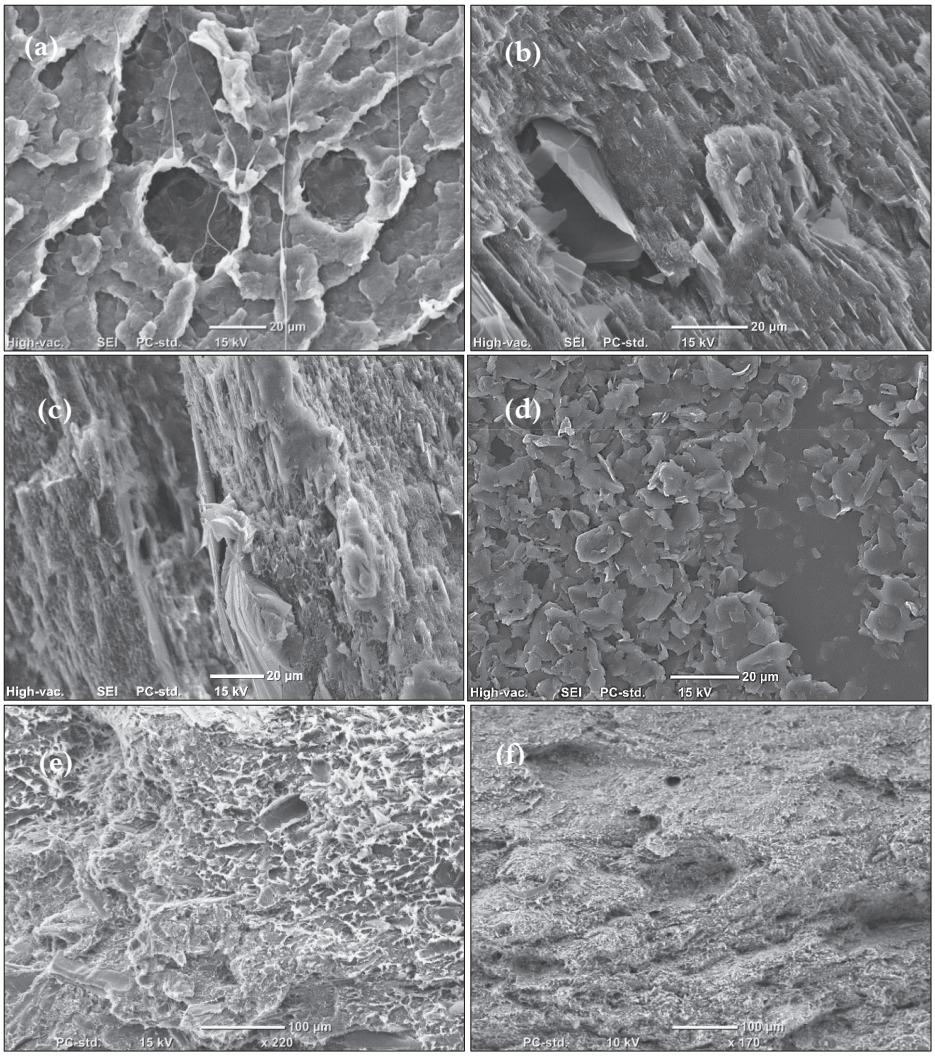

Figure 4. SEM of fracture surfaces of samples showing the morphology change with the addition of GNP: (a) Neat polymer, (b) PE15-M1, (c) a close-up on a PE6-M1 of a large platelet showing the layered structure, (d) a cluster of agglomerated particles in PE15-M1 (e) fracture surface of 40WPC and f) fracture surface of 40WPC15; (a-d) freeze fractured, (e, f) test fractured.

On the other hand, Figure 4d shows a cluster of platelets agglomerated in one place at 15 wt% GNPs loading. This suggests the greater challenge to disperse the particles at high loadings of nano-reinforcement. Due to the large difference in size scale between the two types of reinforcements (wood and GNPs), it is difficult to examine

the distribution of one without losing information about the other in the image. However, the presence of the nanoparticles is obvious by their effect on the morphology of the fracture surface of the wood samples. The plastic deformation of the matrix (appearing as white protrusions) in the 40WPC are replaced by smoother surface in the 40WPC15 sample.

Figure 5 shows the X-ray microtomography images of samples PE15-M1 and PE15-M2 from different viewing planes (definition of planes is in Figure 1). In general, comparing the GNPs from the two masterbatches, it could be seen that the thickness of the individual platelets is above the nanometer scale since it can be picked up on the experiment scale/resolution level. However, it could also be noticed that there is a very good distribution of the particles within the sample despite the inhomogeneity of the particle size distribution. Without the statistical analysis, visual assessment suggests the differences in the thickness of the platelets between the different masterbatches as the images show thicker platelets for M1 (Figure 5 a). It is worth paying attention that despite the similar possibility for particle restacking in both masterbatches, the 10% reduction in the initial number of layers of M2 with respect to those of M1 would lead to thinner particles in the samples.

Even though the bonding between the matrix and the platelets seem to be very good, since no voids could be detected, some foreign inclusions in the samples have been observed that might have occurred during material processing or from the impurities in the original masterbatch. Such inclusions with the possible weakness points around them (voids) represent a large defect and can cause pre-mature failure of specimens at random locations especially if they were close to the edges. However, from the scatter of values from the different tests, one can assume an even distribution of these inclusions as the scatter seems consistent with the corresponding values. It is worth noting that voids around these inclusions can act as pockets for water to reside in causing higher moisture uptake values.

The directionality in alignment of the GNPs is another observation. They seem to follow the direction of the screw extruder and the compression molding. They mostly align themselves in the in-plane direction. This means possible improved properties

in the longitudinal and transverse directions but not in the out-of-plane direction. Figure 5c shows the CT image from the surface of compression where a significant number of particles are facing that direction. It is possible that the particles did have a random direction after the extrusion but have reoriented themselves during the compression process.

This directionality was further comfirmed by the change in dimensional distortion due to thermal effect on samples at different directions with respect to the compression molding face as seen in Figure 6. There is a large reduction in the dimensional distortion of the sample between the x and z directions (directions are defined in Figure 1). Properties of the samples in the x or y directions are dominated by the properties of the platelets while polymer properties are dominating in the z direction where the chains have more mobility and the layers of the particles are bonded by the weaker van der waals bonds. From the figure it can also be speculated that wood fibers have a prefered orientation similar to that of the GNPs, since the decrease in dimensional distortion is larger in the hybrid composite than it is with the wood or the nanocomposite.

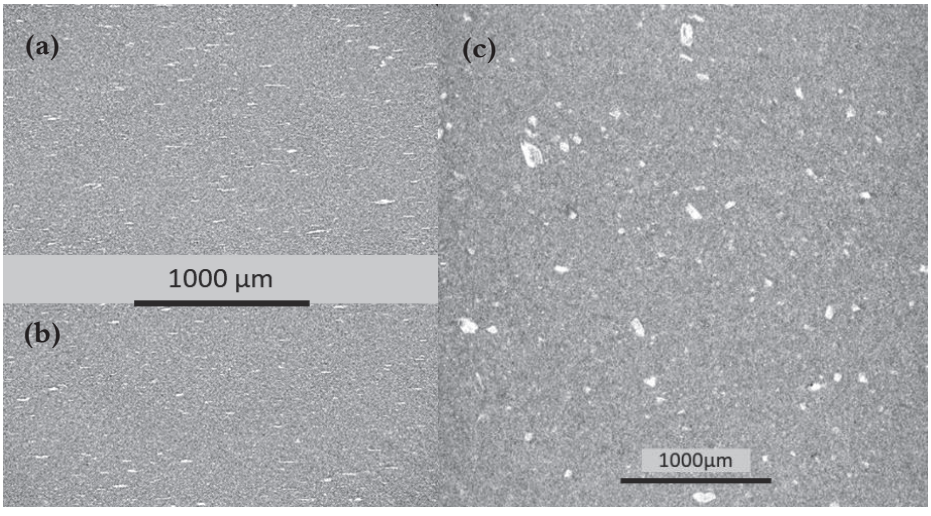

Figure 5. CT micrographs of: (a) PE15-M1 (plane y-z); (b) PE15-M2 (plane y-z); and (c) PE15-M2 (plane x-y).

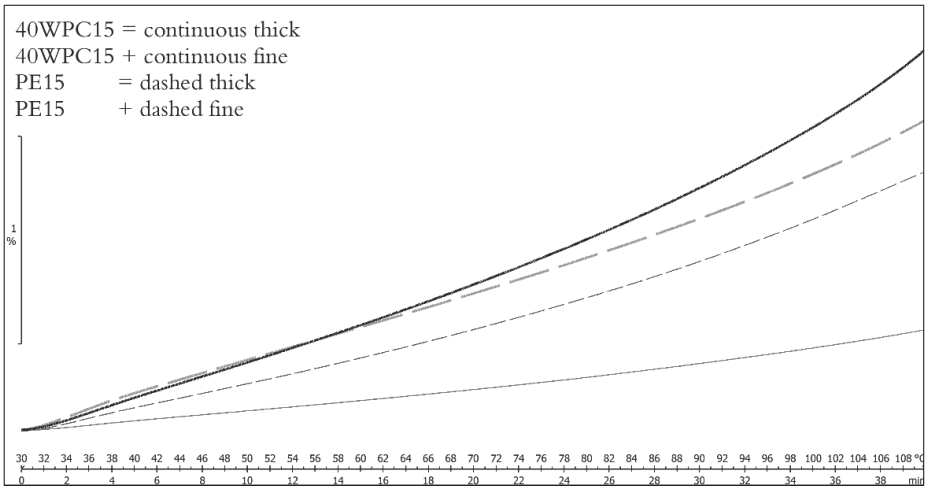

Figure 6. Dimensional distortion dependence on the directionality of the platelets. = represents the distortion in z direction, while + is distortion in x or y directions.

3.4. Moisture Uptake

Figure 7 shows the through-the-thickness moisture absorption curves for the studied materials after 520 hours of conditioning. Despite the clear trend of weight gain with the increased exposure times, this trend in more stable for the wood composites than it is for the nanocomposite. The initial measurements where the moisture uptake is not significant can be easily affected by the equipment/measurement errors. The inevitable exposure of sample to a different environment conditions during weighing might result in diffusion of water molecules to and from the sample depending on the surrounding conditions. This is less pronounced in the wood composites since water mostly reside deeper in the lumen of the fibers and due to the higher moisture uptake in wood composite.

In general, HDPE is known for its high resistance to moisture uptake (0.01-0.03% after direct immersion in water for 24 hours [27]). It seems that the addition of the small amounts of the GNP have a positive effect on this resistance as the tendency to take up moisture is decreased. On the other hand, at higher graphene loadings, possible formation of the agglomerates can result in the micro-voids that act as pockets for water to be absorbed in, and hence the increase in the water content. It

is logical that the presence of wood in the composite increases the moister uptake significantly due to its inherent hydrophilic nature. And this uptake increases with the increased content of WF in the composite.

Since the used graphene is functionalized only at the edges and the molecules at the edges are already bonded to the polymer, a decrease in the water absorption is expected. On the other hand, the bulk of the graphene sheet surface is not functionalized and might result in weaker bonding with the polymer causing voids allowing water to penetrate. It is possible as well that water penetrates through the layers of stacked platelets. Graphene hydrophobicity/hydrophilicity is controversial in literature and recorded behavior depends mostly on the substrate material [28]. Therefore, any difference in the moisture uptake behavior after addition of these particles is most likely attributed to the change in mechanism of water diffusion rather than the hydrophobic/hydrophilic nature of the additives. The particles make new torturous paths against water molecules and act as obstacles delaying their penetration into the polymer.

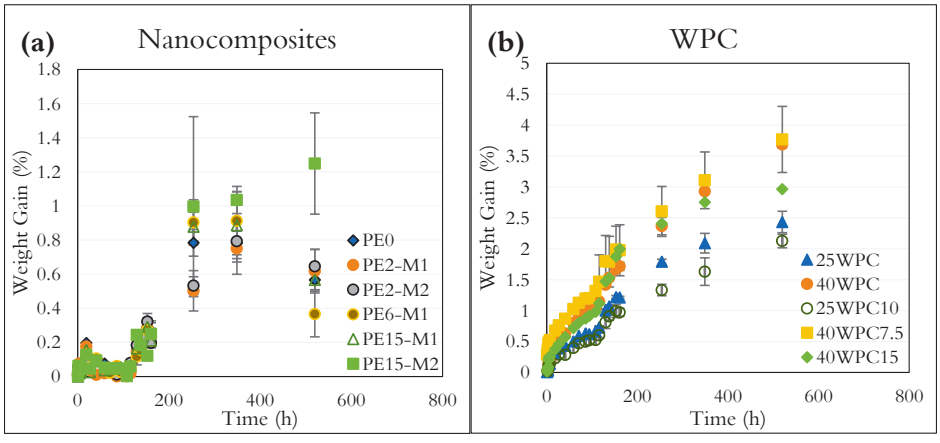

Figure 7. Moisture absorption curves in terms of % weight gain for the nanocomposites (a); and the wood polymer composites (b).

3.5. Flexural Properties

Elevated moisture content in the material might influence its mechanical performance. This was investigated by measuring the flexural properties before and after exposure to moisture. Figure 8 shows representative flexural stress strain curves of the nanocomposite and the WPCs, before and after moisture uptake. In general, trends similar to those observed in the tensile curves are observed here. The materials become stiffer with the increased content of GNPs, and the masterbatch of fewer layer of graphene in the platelets (M2) outperforms the other. For the WPCs, the increase in content of any of the reinforcements lead to increase in the composite performance.

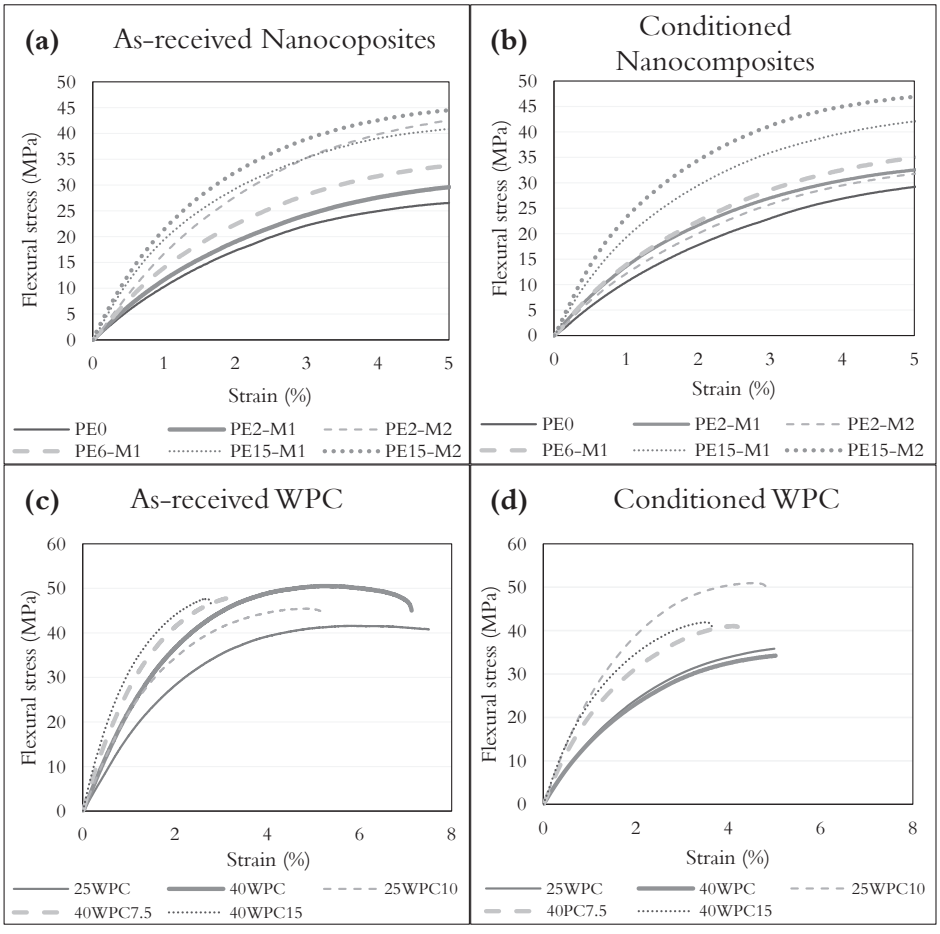

Figure 8. Flexural stress- strain curves of the nanocomposites before (a) and after (b) moisture uptake; and for WPC before (c) and after (d) moisture uptake.

The effect of moisture on the properties of the nanocomposites is not so significant. Except for the sample PE2-M2 where the curve is lower, indicating degraded properties, the general trend seems to be the same and effect of moisture on materials can be regarded as marginal. On the other hand, the moisture effect on WPCs is more pronounced. The moisture-saturated wood in the composite decreases the flexural properties and the presence of the nanoplatelets seems to restrict this effect.

The flexural test fracture surfaces presented in Figure 9 show differences in the failure mechanism. Before conditioning, the surface indicates more brittle fracture and failure appears in form of matrix cracking, while conditioned samples showed failure in terms of fiber sliding (enclosed in ovals) and fiber pull-out as indicated by the deep holes (marked by arrows) in Figure 9. This is possibly because the fibers swell after the moisture uptake creating stress concentrations on the interface leading to these debonds during bending. Indications of some polymer plasticizing could also be noticed on the sliding surfaces of conditioned samples. Figure 10 demonstrates graphically the two important properties of the flexural test showing the effect of moisture uptake while numerical values of the properties obtained by flexural test are presented in Table 4 and Table 5 for the nanocomposite and the WPCs, respectively.

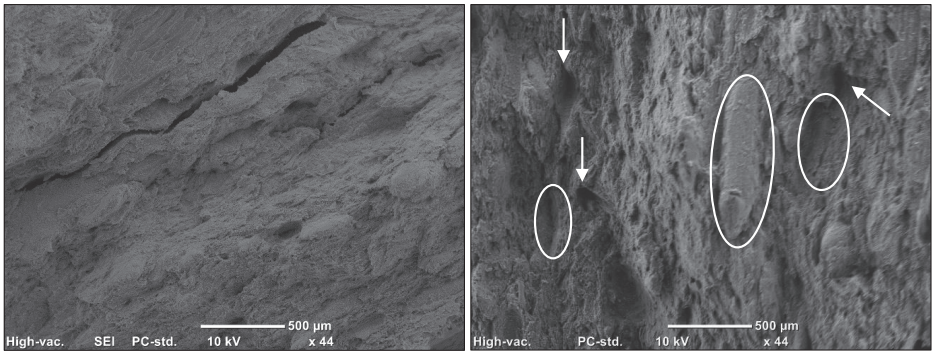

Figure 9. Flexural fracture surface before and after moisture. Left is as-received 40WPC15, right is conditioned 40WPC15 (see significance of the marks in the text).

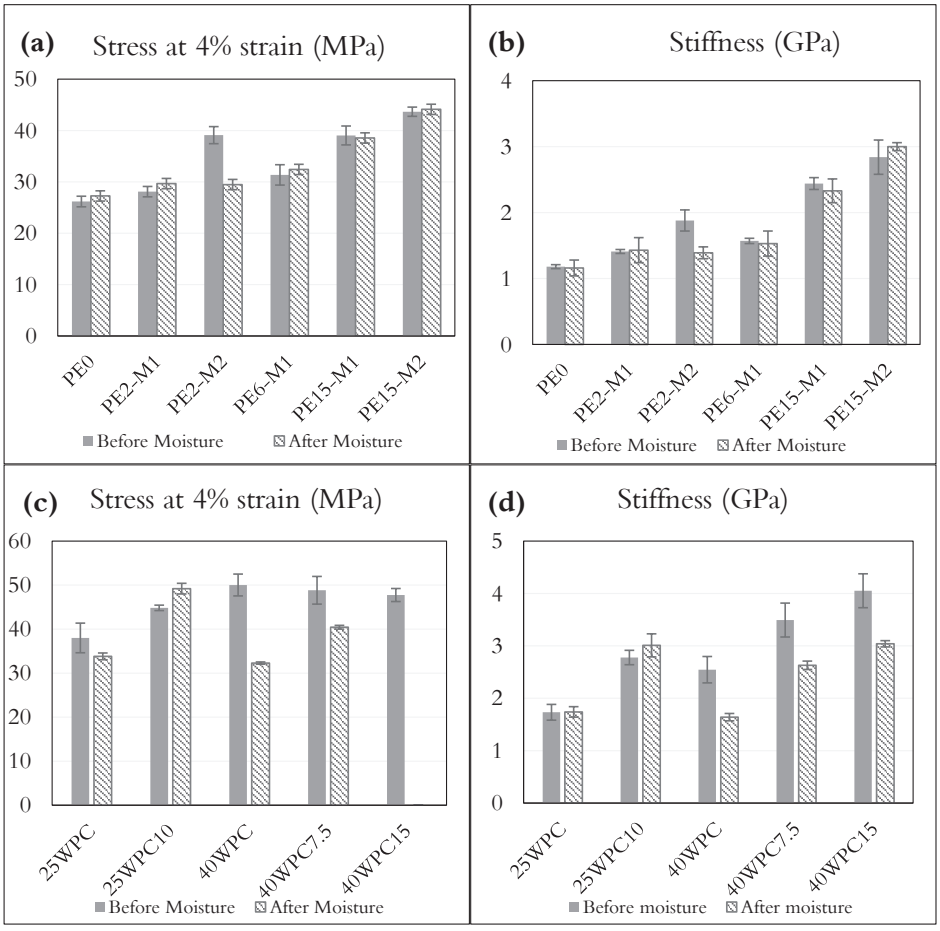

Figure 10. Effect of moisture on the flexural properties of the materials: (a, b) flexural stress and stiffness for the nanocomposites; (c, d) flexural stress and stiffness of WPCs. Sample 40WPC15 broke at average strains below 4% (3.47%) registering an average maximum stress of 41.72 MPa.

Table 4. Flexural properties of the nanocomposites with moisture effect.

Sample	E [std] (GPa)		$^{\star}\sigma_{max}$ [std] (MPa)		$\sigma_{4\%\epsilon}$ [std] (MPa)		$\epsilon_{25\,MPa}$ [std] (%)	
	**AR	**C	AR	C	AR	C	AR	C
PE0	1.18 [0.03]	1.16 [0.12]	28.10 [1.00]	31.14 [0.82]	26.18 [0.81]	27.26 [1.03]	3.61 [0.25]	3.37 [0.24]
PE2-M1	1.41 [0.03]	1.43 [0.19]	30.02 [0.64]	33.68 [0.77]	28.10 [0.61]	29.67 [1.01]	3.06 [0.14]	2.81 [0.24]
PE2-M2	1.88 [0.16]	1.39 [0.09]	NA	33.43 [1.26]	39.10 [1.63]	29.48 [1.66]	1.78 [0.14]	2.88 [0.33]
PE6-M1	1.57 [0.04]	1.53 [0.19]	33.41 [0.48]	36.87 [1.75]	31.36 [0.48]	32.42 [1.98]	2.48 [0.07]	2.44 [0.29]
PE15-M1	2.44 [0.09]	2.33 [0.18]	40.83 [0.42]	42.27 [1.60]	39.04 [0.39]	38.55 [1.84]	1.51 [0.01]	1.65 [0.17]
PE15-M2	2.84 [0.26]	3.00 [0.06]	NA	46.88 [0.78]	43.66 [3.62]	44.12 [0.90]	1.51 [0.01]	1.2 [0.05]

* Max. strength at 5% strain based on standards recommendation. ** AR= as received, C= conditioned.

Table 5. Flexural properties of WPCs with moisture effect.

Sample	E [std] (GPa)		σ_{max} [std] (MPa)		ϵ_{25MPa} [std] (%)	
	*AR	*C	**AR	C	AR	C
25WPC	1.73 [0.15]	1.74 [0.1]	38.00 [3.37]	36.37 [1.12]	1.79 [0.33]	2.14 [0.09]
25WPC10	2.78 [0.14]	3.01 [0.22]	44.83 [0.62]	47.47 [3.51]	1.14 [0.04]	1.08 [0.05]
40WPC	2.55 [0.25]	1.64 [0.07]	50.02 [2.48]	34.61 [0.33]	1.11 [0.11]	2.34 [0.05]
40WPC7.5	3.49 [0.32]	2.63 [0.08]	48.83 [3.15]	40.54 [0.39]	0.87 [0.09]	1.37 [0.03]
40WPC15	4.05 [0.32]	3.04 [0.06]	47.75 [1.48]	41.72 [0.23]	0.73 [0.02]	1.12 [0.04]

* AR= As-Received, C=conditioned. ** Stress at 4% elongation to facilitate comparison of all samples.

3.6. Differential Scanning Calorimetry

Studies have shown both positive and negative impact on crystallinity when adding nanoparticles into the polymers [29,30]. It is possible that there is a competing mechanism that result in one effect or the other such as crystallization rate and heterogeneity of crystallization. Based on the size and distribution of the nanoparticles, they can act as nucleating agent around which spherulites start to form and grow. On the other hand, if these particles are big they can restrict the growth of the crystals and hinder the heterogeneous crystallization [31]. Figure 11 and Table 6 show this competing mechanism.

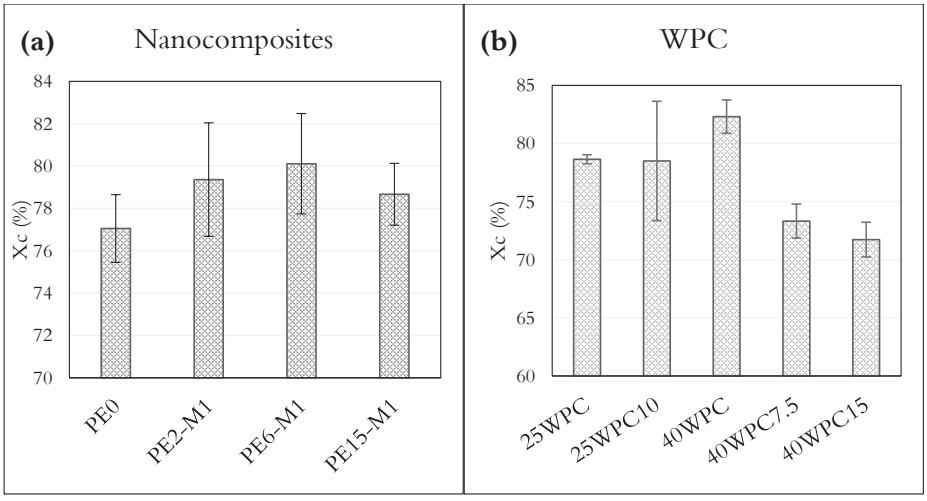

Figure 11. Degree of crystallinity of the tested materials for: (a) the nanocomposites; and (b) the wood polymer composite.

At high filler loading (6 wt% GNP upwards), the crystallization starts earlier in the sample (higher temperature in the cooling stage) but the degree of crystallinity shows no significant change (the change is within the range of error). The presence of both fillers has a more pronounced effect on the crystallization, since the high amount of fillers provide no space for the crystals to grow and hence the crystallinity is decreased (at 40WPC7.5 and 40WPC15). It is worth noting that number of specimens tested was different for the nanocomposite than the WPC and WPC nanocomposite, that

is why the range of scatter values are varying. Additionally, the DSC measurements is sensitive to sample homogeneity and it is difficult to secure a representative sample for the bulk of the material at 5-10 mg weight. This has been investigated for several samples of PE6-M1 in TGA, where the residual mass after 5 random measurements was always less than 6% the initial mass which leads to higher crystallinity if equation (1) is used based on the assumption of homogeneous sample since the amount of polymer is being overestimated.

Table 6. DSC results of the different composites.

Sample	T_O★ [std] (°C)	T_m★ [std] (°C)	T_c★ [std] (°C)	X_c★[std] (%)
PE0	125.41 [0.22]	132.88 [0.97]	114.99 [0.64]	77.05 [1.60]
PE2	124.67 [0.33]	134.53 [0.98]	115.76 [1.28]	79.36 [2.68]
PE6	125.42 [0.34]	133.55 [0.45]	117.04 [0.62]	80.11 [2.37]
PE15	125.23 [0.38]	133.56 [0.45]	117.79 [0.81]	78.67 [1.46]
25WPC	125.64 [0.03]	134.35 [0.11]	117.42 [0.13]	78.65 [0.39]
25WPC10	126.04 [0.44]	132.80 [0.40]	121.06 [0.02]	78.50 [5.13]
40WPC	125.42 [0.05]	134.82 [0.20]	117.27 [0.23]	82.32 [1.43]
40WPC7.5	127.14 [0.04]	135.97 [0.27]	117.68 [0.04]	73.33 [1.46]
40WPC15	125.82 [0.06]	134.67 [0.41]	117.17 [0.00]	71.73 [1.49]

★T_O, T_m, T_c: onset, melting and crystallization temperatures respectively. X_c: degree of crystallinity. [std]: standard deviation.

3.7. Thermal transport properties

Figure 12 shows the thermal conductivity and thermal diffusivity of the samples measured by thermal transient method. The values of the thermal conductivity of the neat polymer is higher than those reported in polymer database [27]. It is possible that the higher crystallinity of the samples result in a better thermal conductivity as the thermal wave can travel in the ordered structure better than the amorphous structure where the vibrational modes are localized [32]. The immediate increase in the thermal conductivity after the addition of the GNPs is attributed to the inherent

high thermal conductivity of GNPs. Similarly, the insolation behavior of the wood flour is apparent in the reduced conductivity of the wood composite with respect to the neat polymer and this reduction is larger with the increased wood content.

There are several factors affecting the phonon transport through the nano-reinforced polymers which complicates the mechanisms of thermal conduction and their understanding. Some of these factors are the phonon scatter at the weak interfaces and the size of the conductive particles that affect the size of the contact area, chemical composition and the alignment of the polymer chains etc. [32]. Many of these factors may play role in altering the thermal conductivity of the materials in this study. For example, the gradient of crystallinity through the sample thickness as a result of the immediate exposure of the demolded surface (quenching) after compression molding compared to the gradual cooling deeper in the sample. The noticed and discussed alignment of the particles should result in anisotropic conductivity in contrast to the assumed isotropic behavior during test setup.

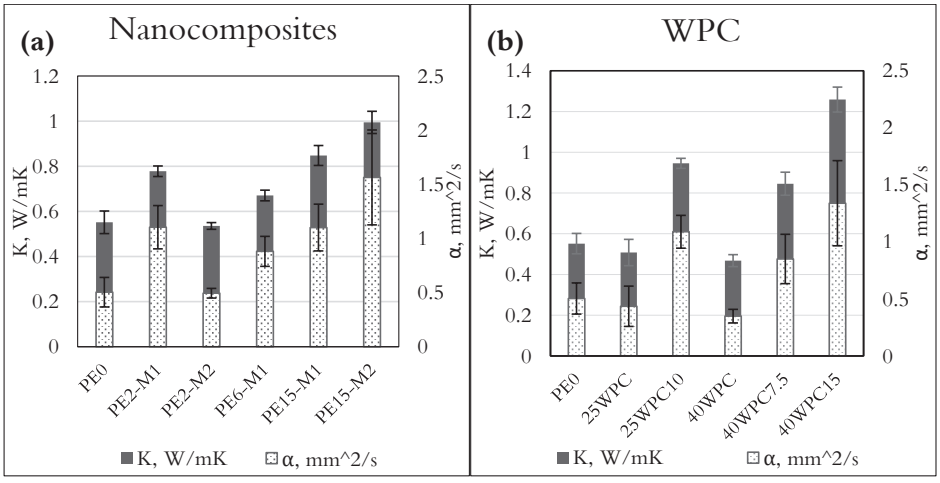

Figure 12. Thermal conductivity and diffusivity of the nanocomposites (a); and the wood polymer composite (b).

The synergistic effect of the two types of reinforcement is observed by the improved thermal behavior of the hybrid composite at the same amount of conductive filler

(40WPC15 and PE15-M1 which are made of the same GNP type). The presence of wood leads to increase in both the thermal conductivity and thermal diffusivity. This can be directly explained by the formation of conductive paths aided by the presence of wood as a scaffold for formation of particle network. Once again, the samples made with the masterbatch M2 outperform that of M1 which has more scattering sites dictated by the higher number of layers.

4. Conclusions

Modification of HDPE was achieved using high content HDPE-based graphene masterbatch with two types of GNP. The masterbatch with fewer layer graphene sheets in the platelets showed better performance compared to the thicker platelets. Improvement in the mechanical properties to a maximum of 140% and 79% was achieved for the tensile stiffness and stress at yield at 15 wt% GNPs. Composites with hybrid reinforcements (GNP and woof flour) showed an improvement in the flexural properties of 243% in terms of bending stiffness and the addition of GNPs restricted the reduction of stiffness due to moisture. Results also showed a preferred direction of reinforcement alignment by the effect of the processing method. Moreover, improved thermal conductivity was measured for the modified composites which makes them candidates for applications like thermal management of buildings.

Acknowledgement

This study is financially supported by Interreg Nord project "Smart WPC" (funded by European Union and Region Norrbotten).

Authors would like to thank Runar Långström and Robert Westerlund at RISE SICOMP for extrusion and compression molding the composites, and Vanessa Meulenberg and Lena Brunnaker (project students within T7009T course at LTU) for help with experiments. Special thanks for Jevgeniys Sevcenko at the institute of mechanics of materials (Riga, Latvia) for running the TMA experiment.

Support in kind provided by partners within NANO2DAY project (Grant agreement ID: 777810 funded under H2020-EU) is highly appreciated by the authors.

References

[1] S. Araby, Q. Meng, L. Zhang, H. Kang, P. Majewski, Y. Tang, J. Ma, Electrically and thermally conductive elastomer/graphene nanocomposites by solution mixing, Polym. (United Kingdom). 55 (2014) 201–210. doi:10.1016/j.polymer.2013.11.032.

[2] Grand View Research, Graphene Market Size , Share & Trends Analysis Report By Application (Electronics , Composites , Energy), By Product (Graphene Nanoplatelets , Graphene Oxide), By Region , And Segment Forecasts , 2019 - 2025, 2019.

[3] P. Kiran, S. Chakrabort, Graphene Market Size By Product (Graphene Oxide, Graphene Nanoplatelets, Mono-layer & Bi-layer Graphene), By End-user (Electronics, Aerospace & Defense, Energy, Automotive, Healthcare), Industry Analysis Report, Regional Outlook (U.S., Canada, Germany, UK, 2017.

[4] M. Keramati, I. Ghasemi, M. Karrabi, H. Azizi, M. Sabzi, Incorporation of surface modified graphene nanoplatelets for development of shape memory PLA nanocomposite, Fibers Polym. 17 (2016) 1062–1068. doi:10.1007/s12221-016-6329-7.

[5] X. Zhao, Q. Zhang, D. Chen, P. Lu, Enhanced mechanical properties of graphene-based polyvinyl alcohol composites, Macromolecules. 43 (2010) 2357–2363. doi:10.1021/ma902862u.

[6] H. Bin Zhang, W.G. Zheng, Q. Yan, Y. Yang, J.W. Wang, Z.H. Lu, G.Y. Ji, Z.Z. Yu, Electrically conductive polyethylene terephthalate/graphene nanocomposites prepared by melt compounding, Polymer (Guildf). (2010). doi:10.1016/j.polymer.2010.01.027.

[7] K. Wakabayashi, C. Pierre, D.A. Diking, R.S. Ruoff, T. Ramanathan, L. Catherine Brinson, J.M. Torkelson, Polymer - Graphite nanocomposites: Effective dispersion and major property enhancement via solid-state shear pulverization, Macromolecules. (2008). doi:10.1021/ma071687b.

[8] A. Dasari, Z.Z. Yu, Y.W. Mai, Electrically conductive and super-tough polyamide-based nanocomposites, Polymer (Guildf). (2009). doi:10.1016/j.polymer.2009.06.026.

[9] A.J. Bourque, C.R. Locker, A.H. Tsou, M. Vadlamudi, Nucleation and mechanical enhancements in polyethylene-graphene nanoplate composites, Polym. (United Kingdom). 99 (2016) 263–272. doi:10.1016/j.polymer.2016.07.025.

[10] E. Tarani, Z. Terzopoulou, D.N. Bikiaris, T. Kyratsi, K. Chrissafis, G. Vourlias, Thermal conductivity and degradation behavior of HDPE/graphene

nanocomposites: Pyrolysis, kinetics and mechanism, J. Therm. Anal. Calorim. 129 (2017) 1715–1726. doi:10.1007/s10973-017-6342-0.

[11] X. Zhang, X. Hao, J. Hao, Q. Wang, Heat transfer and mechanical properties of wood-plastic composites filled with flake graphite, Thermochim. Acta. (2018). doi:10.1016/j.tca.2018.04.003.

[12] S. Sheshmani, A. Ashori, M. Arab Fashapoyeh, Wood plastic composite using graphene nanoplatelets, Int. J. Biol. Macromol. 58 (2013) 1–6. doi:10.1016/j.ijbiomac.2013.03.047.

[13] M. Miao, C. Wei, Y. Wang, Y. Qian, Effect of Compatibilizer on the Interface Bonding of Graphene Oxide/Polypropylene Composite Fibers, Polymers (Basel). (2018). doi:10.3390/polym10111283.

[14] G. Gong, Literature study of graphene modified polymeric composites, Piteå, 2018.

[15] H. Kim, Y. Miura, C.W. MacOsko, Graphene/polyurethane nanocomposites for improved gas barrier and electrical conductivity, Chem. Mater. (2010). doi:10.1021/cm100477v.

[16] R. Verdejo, M.M. Bernal, L.J. Romasanta, M.A. Lopez-Manchado, Graphene filled polymer nanocomposites, J. Mater. Chem. (2011). doi:10.1039/c0jm02708a.

[17] K. Singh, A. Ohlan, S.K. Dhaw, Polymer-Graphene Nanocomposites: Preparation, Characterization, Properties, and Applications, in: Nanocomposites - New Trends Dev., 2012. doi:10.5772/50408.

[18] A.A. Vasileiou, M. Kontopoulou, A. Docoslis, A noncovalent compatibilization approach to improve the filler dispersion and properties of polyethylene/graphene composites, ACS Appl. Mater. Interfaces. (2014). doi:10.1021/am404979g.

[19] C. Punckt, F. Muckel, S. Wolff, I.A. Aksay, C.A. Chavarin, G. Bacher, W. Mertin, The effect of degree of reduction on the electrical properties of functionalized graphene sheets, Appl. Phys. Lett. (2013). doi:10.1063/1.4775582.

[20] S. Park, S. He, J. Wang, A. Stein, C.W. Macosko, Graphene-polyethylene nanocomposites: Effect of graphene functionalization, Polymer (Guildf). (2016). doi:10.1016/j.polymer.2016.09.058.

[21] B.D. Boscia, D.J. Arthur, A. Wagner, Nanocomposite master batch composition and method of manufacture, US8124678B2, 2012.

[22] J.H. Ding, H.R. Zhao, H. Bin Yu, A water-based green approach to large-scale production of aqueous compatible graphene nanoplatelets, Sci. Rep. (2018). doi:10.1038/s41598-018-23859-5.

[23] R.L. Blaine, Thermal Applications Note - Polymer Heats of Fusion, Therm. Appl. Note. (2002).

[24] S. Lin, M.A.S. Anwer, Y. Zhou, A. Sinha, L. Carson, H.E. Naguib, Evaluation of the thermal, mechanical and dynamic mechanical characteristics of modified graphite nanoplatelets and graphene oxide high-density polyethylene composites, Compos. Part B Eng. (2018). doi:10.1016/j.compositesb.2017.08.010.

[25] N. Domun, K.R. Paton, H. Hadavinia, T. Sainsbury, T. Zhang, H. Mohamud, Enhancement of fracture toughness of epoxy nanocomposites by combining nanotubes and nanosheets as fillers, Materials (Basel). (2017). doi:10.3390/ma10101179.

[26] S. Chandrasekaran, N. Sato, F. Tölle, R. Mülhaupt, B. Fiedler, K. Schulte, Fracture toughness and failure mechanism of graphene based epoxy composites, Compos. Sci. Technol. (2014). doi:10.1016/j.compscitech.2014.03.014.

[27] CROW, Polymer Properties Database, Polymerdatabase.Com. (2016). https://polymerdatabase.com/Commercial Polymers/HDPE.html (accessed April 14, 2019).

[28] L.A. Belyaeva, P.M.G. van Deursen, K.I. Barbetsea, G.F. Schneider, Hydrophilicity of Graphene in Water through Transparency to Polar and Dispersive Interactions, Adv. Mater. (2018). doi:10.1002/adma.201703274.

[29] S. Lee, J.Y. Hong, J. Jang, The effect of graphene nanofiller on the crystallization behavior and mechanical properties of poly(vinyl alcohol), Polym. Int. (2013). doi:10.1002/pi.4370.

[30] P. Xu, X. Luo, Y. Zhou, Y. Yang, Y. Ding, Enhanced cold crystallization and dielectric polarization of PLA composites induced by P[MPEGMA-IL] and graphene, Thermochim. Acta. 657 (2017) 156–162. doi:10.1016/j.tca.2017.10.005.

[31] K. Müller, E. Bugnicourt, M. Latorre, M. Jorda, Y. Echegoyen Sanz, J. Lagaron, O. Miesbauer, A. Bianchin, S. Hankin, U. Bölz, G. Pérez, M. Jesdinszki, M. Lindner, Z. Scheuerer, S. Castelló, M. Schmid, Review on the Processing and Properties of Polymer Nanocomposites and Nanocoatings and Their Applications in the Packaging, Automotive and Solar Energy Fields, Nanomaterials. (2017). doi:10.3390/nano7040074.

[32] C. Huang, X. Qian, R. Yang, Thermal conductivity of polymers and polymer nanocomposites, Mater. Sci. Eng. R Reports. 132 (2018) 1–22. doi:10.1016/j.mser.2018.06.002.

Paper III

Effect of Nano-reinforcement on the Time-dependent Properties of Graphene Modified High Density Polyethylene

Liva Pupure, Zainab Al-Maqdasi, Guan Gong, Nazanin Emami and Roberts Joffe

Original Research Paper

Effect of Nano-reinforcement on the Time-dependent Properties of Graphene Modified High Density Polyethylene

Liva Pupure[1], Zainab Al-Maqdasi[1], Guan Gong[2], Nazanin Emami[1], and Roberts Joffe[1]

[1]Luleå University of Technology, SE 97187 Luleå, Sweden
[2]RISE SICOMP AB, SE 94126 Piteå, Sweden

Abstract

Viscoplasticity using Zapas model has been analyzed for high-density polyethylene (HDPE) reinforced with 2, 6 and 15 wt% graphene nanoplatelets, as well as pure HDPE as a reference material. Viscoelastic behavior has also been investigated in this paper by comparing creep curves and creep compliance curves. In addition, morphological changes in the materials upon the addition of the different amounts of the platelets have been investigated by scanning electron microscope. The obtained results showed that only reinforcement of 15 wt% GNP showed significant effect on time-dependent behavior, reducing the strain approximately 2 times. The creep compliance curves showed that nano-reinforced HDPE behaves nonlinearly viscoelastic even at very low stress levels.

Keywords: Viscoelastic, viscoplastic, creep, graphene nanoplatelets (GNPs), high density polyethylene (HDPE)

1. Introduction

Polymers and their composites are gaining increased interest as alternative, light-weight solutions replacing metals in variety of applications. Moreover, with development of nano-technology, new multi-scale, multi-functional polymeric materials with nano-scaled reinforcements are being designed and research continues to characterize their physical, thermal and mechanical properties. Of these materials, polymers doped with nano-scale carbon derivatives (e.g. fullerenes, diamonds, carbon nanotubes and graphene) are emerging as candidates for automotive and other more advanced applications. Due to the large aspect ratio of these nano-materials (at least one dimension is below 100 nm while other dimensions are usually in the microscale), notable improvement in mechanical properties of the polymers has been realized [1]. One of the main advantages of reinforcing the polymer with these nano-sized particles is the percent of improvement achieved with almost no compromise in weight.

It has been shown that even polymers with nano-reinforcement exhibit nonlinear behavior, but research on time-dependent properties of these materials is still limited [2,3], and thus conclusions are not firmly established. Incorporation of nano-reinforcements has been shown to reduce the degree of nonlinearity in the viscoelastic behavior of the thermoplastic Polyamide 66 (PA66) where smaller size of particles was found to contribute in better improvement in their creep resistance [4]. Not only the size of the particles, but also their shape [5] and volume fraction [6] are reported to influence the creep response of the nanocomposites. Among the different morphologies of carbon nano-additives (carbon black, carbon nanotubes and graphene sheets), graphene sheets were reported to have the highest positive influence on the creep resistance of the host polymer [11]. On the other hand, negligible effect on the creep behavior of thermoset epoxy matrix has been observed after reinforcing with e.g. multi-wall carbon nanotubes [7]. Further research shows that at low temperatures or small loads at elevated temperatures, CNTs contributed to enhanced creep resistance of glass fiber epoxy systems compared to unreinforced systems [8].

One of the phenomena which is crucial for performance of materials over time is development of irreversible deformation caused by microdamage or viscoplasticity. The mechanism of altering the time-dependent response by the incorporation of nano-reinforcement is best explained by the restricted mobility of polymer chains by the effect of rigid inclusions.

Modelling and prediction of response of material over time help avoiding extensive time-consuming tests. Conventional models used for the prediction of time-dependent response in viscoelastic materials are the empirical models such as Norton power law and its modifications or constitutive models in which damage accumulations are considered and extensive experiments for parametric identification are avoided [9]. However, it is important to find models that accurately describe the new class of nano-reinforced materials. Special for these nano-reinforcements is the difficulty to disperse them in the resin system (they tend to restack and aggregate) for full exploitation of their reinforcing potential. Therefore, not all models can work properly in describing the behavior of inhomogeneous materials [10].

The purpose of this study is to look into time-dependent performance of high-density polyethylene (HDPE) doped with graphene nanoplatelets (GNPs) - material developed in **Paper II**. The focus of the paper is on characterization of non-linear behavior of these materials and identification of parameters representing time-dependent properties. One of the tasks is also evaluation of applicability of earlier developed models to predict creep of nanocomposites as well as validation of modeling approach in general for these types of materials. This is done by performing experimental characterization of irreversible i.e. viscoplastic (VP) strain development and identifying VP model based on these measurements.

The VP model used in this study is suggested by Zapas et. al [12] and has been successfully used to describe VP strain development in several materials [13–17]. In this model, the VP strain is written in form of stress dependent integral, with parameters determined in creep and strain recovery tests (the applicability of this model is also verified in the suggested testing methodology). Quantitative analysis of effect of GNPs on viscoelasticity of HDPE has also been performed.

2. Experimental

High-density Polyethylene (HDPE) (MG9647S, BOREALIS) pellets was used for matrix material. An HDPE-based masterbatch containing 35 wt% graphene nanoplatelets (GNPs) (heXo HDPE1-V20/35, NanoXplore) was used to incorporate GNP into the HDPE matrix. The GNP in the masterbatch are platelets of 40 layers graphene functionalized at the edges to enhance their compatibility with the polymer. No additional coupling agent or compatibilizer was used in the resulting composites. The composites were manufactured by melt compounding in a co-rotating twin screw extruder (ZSK25, Krupp Wener & Pfleiderer GmbH) followed by compression molding using a conventional 310-ton press (Fjellman). Specimens were cut from the pressed plates using waterjet, and thoroughly dried prior to any test. Details of the composite processing could be found in a previous publication [18], which will not be elucidated here. The content of GNP in the resulting composites were 2, 6, and 15 wt%, respectively. Neat HDPE matrix was used as reference material for comparison.

To demonstrate morphology of the prepared materials, scanning electron microscopy (SEM, JEOL JCM-6000 Neoscope) with electron acceleration of 15 kV was performed. Samples were broken in liquid nitrogen, and the fractured surface was sputter-coated with gold prior to the microscopic study.

Creep tests (in tension) were performed on electromechanical tensile machine Instron 3366 equipped with 10 kN load cell and pneumatic grips following the test sequence presented in Figure 1. Standard Instron extensometers 2620-601 with 50 mm base was used to measure axial strains ε_x,whereas lateral strains $\varepsilon_y$were measured by strain gages. Specimens (70 mm in gauge length, 18 mm in width) were subjected to sequence of tensile loading ramps each consisting of uploading to constant stress (loading was done in displacement-controlled mode with a rate of 3.5 mm/min which corresponds to a strain rate of 5 %/min); keeping the stress constant for a fixed time (creep); unloading (the same rate as loading) the specimen and waiting for viscoelastic strain recovery (to measure residual strains). The duration of creep in a ramp was 10, 20, 30 and 60 min., with a total creep test time of two hours. The applied stress levels in creep test were 7.5, 10, 12.5 and 15 MPa. Tests were

performed in increasing order of the applied stress to minimize influence of damage on results. After each loading period in the ramp, recovery period followed, which was ×8 longer than the loading time. During strain recovery, the load was kept constant at 4 N. The specimen was not unloaded entirely (to zero load) due to limitations of the equipment.

At the end of the recovery, residual strains in two directions, ε_x^{VP} (further in the paper referred to as axial) and ε_y^{VP} (denoted as lateral), were considered as viscoplastic.

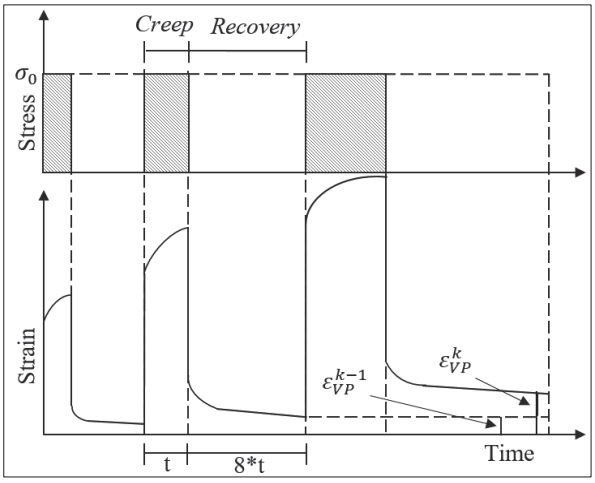

Figure 1. Schematic represents the test sequence and strains at the end of a step k.

3. Modelling of Nonlinear Deformation Behavior

The viscoplasticity was characterized using Zapas and Crissman model [12], where VP strain growth during loading with specified time dependence of the applied stress is given by:

$$\varepsilon_{VP}(\sigma, t) = C_{VP}\left\{\int_0^{\frac{t}{t^*}} \left(\frac{\sigma(\tau)}{\sigma *}\right)^M d\tau\right\}^m \quad \text{(E1)}$$

where C_{VP}, M and m are constants to be determined experimentally, $\sigma*$ is arbitrary chosen stress level, t/t^* is normalized time where t^* is an arbitrary chosen characteristic time constant. In this study, values of $\sigma*$=1 MPa and t^*=7200 s were used.

Limited material was available for this study and thus, methodology described in [16] was employed in order to obtain the maximum amount of information for experimental material constants, with less specimens.

This method allows full characterization of viscoplasticity using only one specimen. Due to the previous loading history, the parameter identification becomes more complicated. At k-th stress level $n_k\sigma_0$ (for the first stress level the n_1=1) and with the same total duration time of creep Δt_0 for previous stress levels, VP strain can be obtained as follows:

$$\varepsilon_{VP}(n_k,t) = C_{VP} \cdot \sigma_0^{mM}\left(\frac{\Delta t_0}{t^*} + n_2^M\frac{\Delta t_0}{t^*} + n_3^M\frac{\Delta t_0}{t^*} + \cdots + n_k^M\frac{t-(k-1)\Delta t_0}{t^*}\right)^m \quad \text{(E2)}$$

Since t^* is an arbitrary chosen constant, the choice of $t^* = \Delta t_0$ reduces equation (E2) to:

$$\varepsilon_{VP}(n_k,t) = C_{VP} \cdot \sigma_0^{mM}\left(1 + n_2^M + n_3^M + \cdots + n_k^M\frac{t-(k-1)\Delta t_0}{t^*}\right)^m \quad \text{(E3)}$$

Applying natural logarithm of both sides of equation (E3) renders the following relationship:

$$ln\left(\varepsilon_{VP}(n_k,t)\right) = ln(C_{VP}\cdot\sigma_0^{mM}) + m \cdot ln\left(1 + n_2^M + n_3^M + \cdots + n_k^M\cdot\frac{t-(k-1)\Delta t_0}{t^*}\right) \quad \text{(E4)}$$

From this equation follows that experimental relationship between VP strain and time $ln(\varepsilon_{VP}) \sim ln\big(f(n_i, M, t)\big)$ has to be linear for all stress levels. Thus, the first step is to find *M* value when for all the stress levels the data points are "linearized". These data can be fitted with function $y = mx + c$, thus obtaining first approximation of parameter *m* and C_{VP}. By further adjusting the parameters, to obtain best overall fit (*m*, C_{VP} values has to be the same for all stress levels), the correct values for viscoplasticity law can be obtained.

Afterwards the VP strain can be subtracted from total amount of strain to obtain pure VE strain. The VP strain was removed with method described in [13]. This methodology allows to use actual VP strain of experiment in subtraction process, thus reducing the effect of scatter between different experiments. The amount of VP strain removed from each individual test will be the same as experimentally measured.

During first creep loading step, viscoplasticity will be removed with following expression:

$$\varepsilon_{VP}^{1}(t) = \varepsilon_{VP}^{c}\left(\frac{t}{\Delta t_1}\right)^{m} \tag{E5}$$

where ε_{VP}^{c} is the VP strain accumulated during loading of first step with total duration of Δt_1. Afterwards, due to previous loading history, removal of viscoplasticity is done according to this expression:

$$\varepsilon_{VP}^{k}(t) = \left\{(\varepsilon_{VP}^{k-1})^{1/m} + [(\varepsilon_{VP}^{k})^{1/m} - (\varepsilon_{VP}^{k-1})^{1/m}]\frac{t - t_{k-1}}{t_k - t_{k-1}}\right\}^{m} \tag{E6}$$

where t_{k-1} is the beginning of current loading step and t_k is the end of current loading step.

4. Results and discussions

Figure 2 shows the morphology of the studied materials at different GNP loadings as seen under the SEM. There is a clear change in the morphology of the polymer from the topological fibrillated surface of the HDPE (and that of the 2 wt% GNP) to the smoother surface at higher GNP loadings (6 wt% and 15 wt%). At 2 wt% GNP, the introduced particles could be detected at some sites (e.g. the one marked with the circle), but the occurrence of GNP is denser on samples of 6 wt% and 15 wt% GNP contents. The platelets appear mostly thin and transparent indicating well exfoliated sheets, but also thicker less exfoliated particles could be spotted. However, they are in general well embedded in the matrix with quite homogeneous distribution. The incorporation of the large rigid GNP in the polymer matrix would restrict the mobility of the polymer chains and cause the material to be more resistant to deformation.

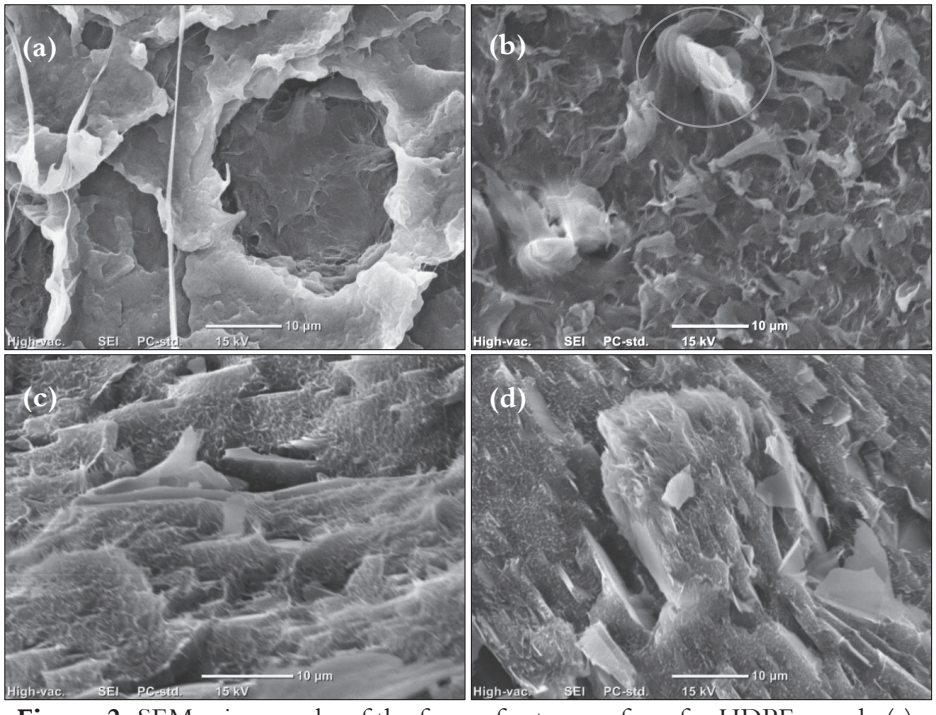

Figure 2. SEM micrographs of the freeze-fracture surfaces for HDPE sample (a), and HDPE at different GNPs; 2 wt% (b), 6 wt% (c) and 15 wt% (d).

VP parameters for axial and lateral direction for all materials are presented in Table 1. It can be seen that parameter *m*, which shows how VP strain develops with time in axial direction, does not change with addition of GNP. Thus, indicating that the time-dependence for all materials is the same in axial direction. The parameters which show how VP strain changes with applied stress level, however, are significantly different for all materials.

In lateral direction the trend is similar, with exception of HDPE + 6 wt% GNP. This could be due to failure of specimen and strain gauge which happened during last loading step of 60 min at 12.5 MPa. It has been seen that fitting of data at higher stress levels is significant for more accurate VP parameter identification.

Table 1. VP parameters in axial and lateral directions for HDPE with different amounts of GNP

Material	Axial			Lateral		
	m	*M*	C_{VP}, %	*m*	*M*	C_{VP}, %
HDPE	0.13	25	$3.29 \cdot 10^{-4}$	0.11	19	$3.05 \cdot 10^{-3}$
HDPE+2%GNP	0.12	30	$1.29 \cdot 10^{-4}$	0.09	36	$1.54 \cdot 10^{-4}$
HDPE+6%GNP	0.13	23	$6.46 \cdot 10^{-4}$	0.22	11	$1.65 \cdot 10^{-3}$
HDPE+15%GNP	0.13	23	$2.47 \cdot 10^{-4}$	0.115	25	$2.13 \cdot 10^{-4}$

The trend for VP strain development for all stress levels was similar. In Figure 3, the VP strains at 12.5 MPa stress level for axial and lateral direction is presented. It can be seen that material with addition of 15 wt% GNP shows the lowest amount of VP strain. It should be noted that the same trend could be observed for both axial and lateral direction and for all applied stress levels. All other materials did not show any significant changes in amount of VP strain at the same stress level and loading time. The maximal difference between lateral VP strain was observed at 12.5 MPa, where HDPE+2wt%GNP showed slightly lower values. The rest of the stress levels showed similar trend as in axial direction. It could also be seen that the specimen of 6 wt% GNP is not following the trend of reduced VP strains. This could be due to some

defects in the particular sample that it is showing higher VP strains compared to the neat polymer or the sample of 2 wt% GNP.

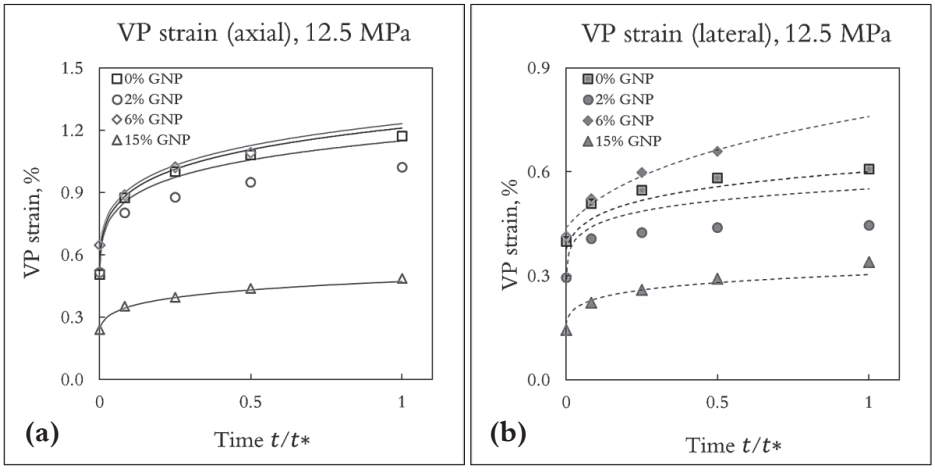

Figure 3. VP strain development with time for HDPE with different amount of GNP at 12.5 MPa applied stress for a) axial and b) lateral direction. Symbols represent experimental data points, lines represent modeling of VP strain.

After viscoplasticity has been analyzed, it is possible to subtract it from the total strain, in order to obtain pure VE strain. The curves for VE strain development for HDPE + 2 wt% GNP at 15 MPa applied stress level is presented in Figure 4 and creep compliance for all the different loading steps also at 15 MPa stress level is presented in Figure 5. It can be seen that for all the loading time durations, the VE strain follows the same curve and similar trend can be observed with creep compliances. This trend was observed for all stress levels. This indicates good repeatability of the experiment. It should be noted that smaller offsets of this trend could be observed at higher stress levels and for lateral strain (as seen in Figure 4b) and Figure 5 b)). Overall the same trend could be observed with all the materials and all stress levels but for the sake of the space only data for stress level of 15 MPa are presented here.

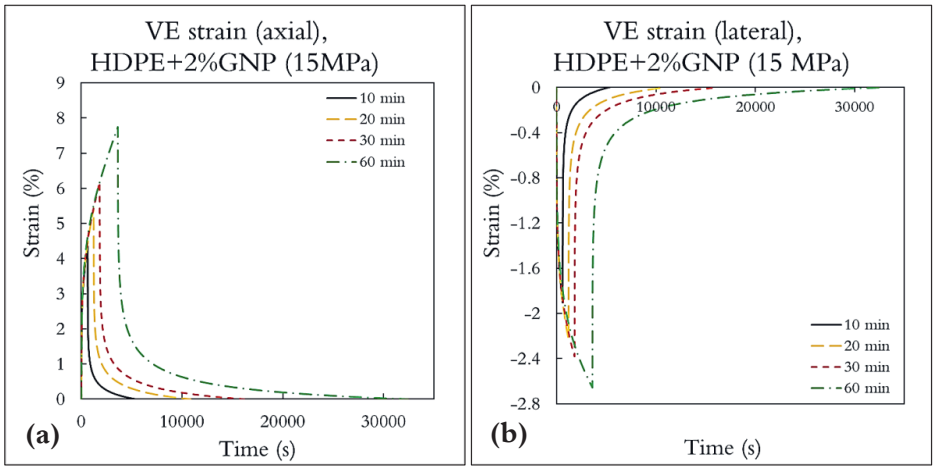

Figure 4. Pure VE strain development with time for HDPE + 2 wt% GNP for different loading durations at 15MPa applied stress level in: (a) axial direction; and (b) lateral direction.

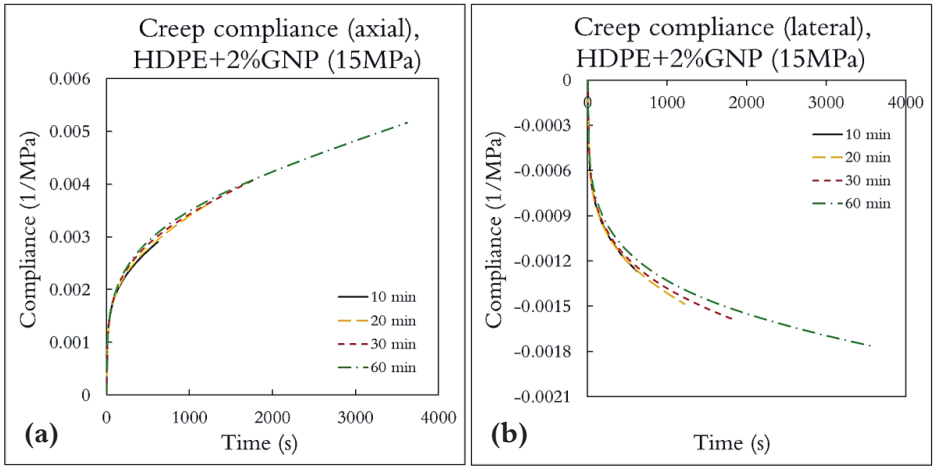

Figure 5. Creep compliance curves for HDPE + 2 wt% GNP for different loading durations at 15 MPa applied stress level in: (a) axial direction; and (b) lateral.

Comparison between different stress levels of pure VE strain and creep compliances for HDPE + 15 wt% GNP are shown in Figure 6 and Figure 7. It can be observed that with increase of applied creep stress the VE strain curves are steeper and with much higher values. The data of creep compliances indicate that even at very low stress level of 10 MPa, the material is nonlinearly viscoelastic, thus modeling of

viscoelasticity for such materials must be performed with nonlinear VE models, e.g., Schapery type of model [19–21]. The same trend was observed for all the materials. It should be noted that in lateral direction, the nonlinear VE region for HDPE + 2 wt% was observed only at 15 MPa applied stress and for HDPE there was no nonlinear VE region. But in axial direction all materials behaved nonlinearly VE even at low stress levels (10 MPa).

Comparison of different materials show similar trend as for viscoplasticity as can be seen in Figure 8 and Figure 9, where pure VE strain at 12.5 MPa and creep compliances at 10 MPa are shown. HDPE with 15 wt% GNP shows almost 2 times lower amount of VE strain as pure HDPE in both axial and lateral direction. HDPE and HDPE with 2 wt% GNP did not show any significant difference in amount of VE strain in axial direction. In axial direction HDPE with 6 wt% of GNP showed small decrease of VE strain. This trend was observed for all the stress levels.

In lateral direction, the difference between materials are more pronounced as the stress increases. This can be seen in Figure 10 where the lowest stress level and highest stress level of lateral VE strain are presented.

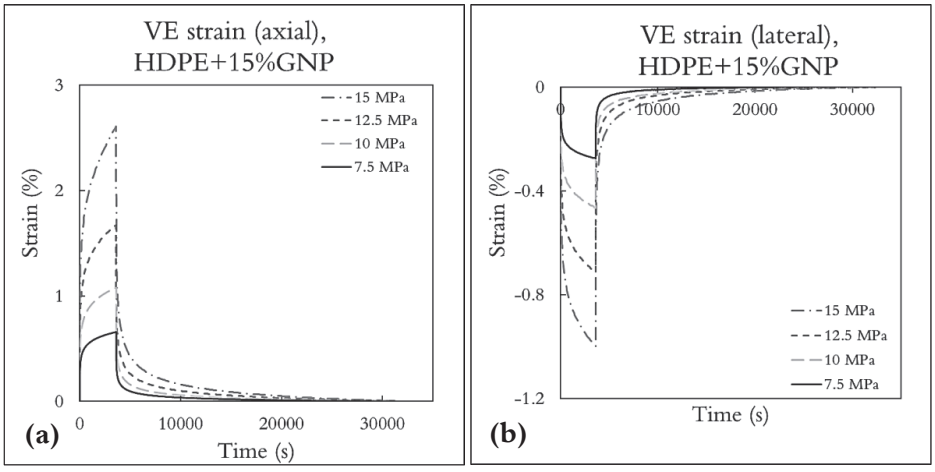

Figure 6. Pure VE strain for HDPE + 15 wt% GNP for different applied stresses for 60 min loading duration in: (a) axial; and (b) lateral direction.

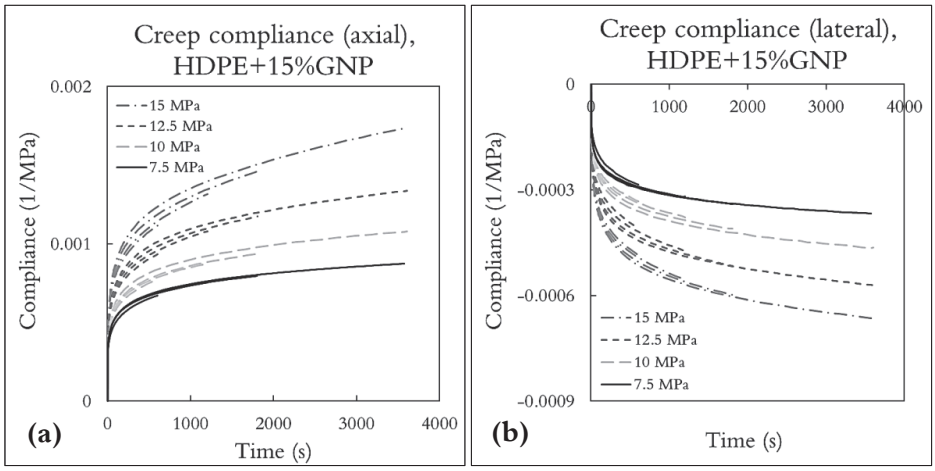

Figure 7. Creep compliances for HDPE + 15 wt% GNP for different applied stresses in (a) axial and (b) lateral direction. Multiple lines correspond to the multiple creep times of individual creep stress.

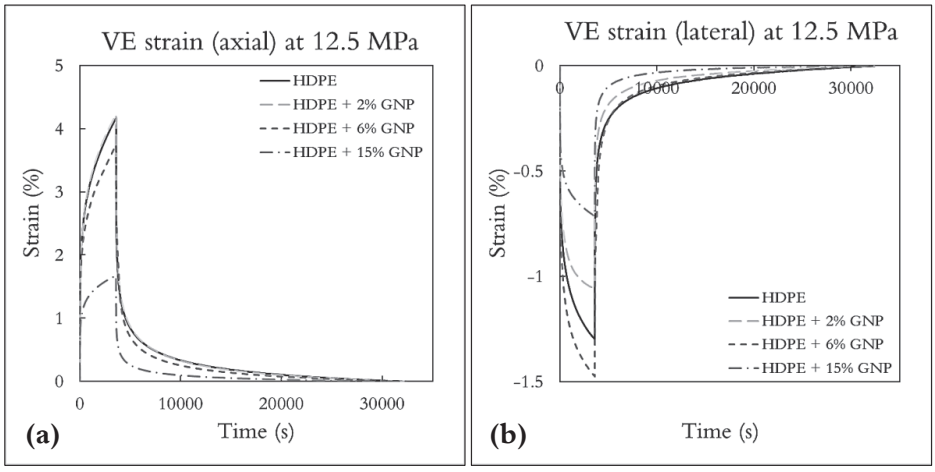

Figure 8. Pure VE strain for HDPE with different GNP content at 12.5 MPa in (a) axial and (b) lateral direction.

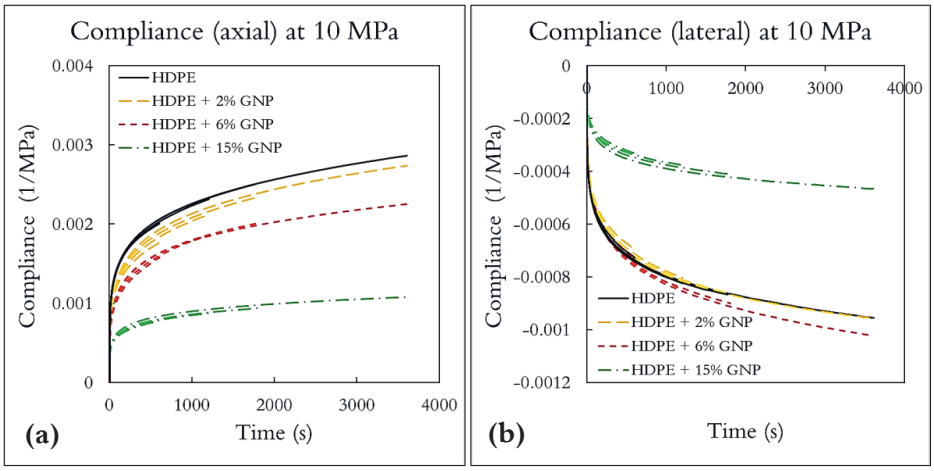

Figure 9. Creep compliances for HDPE with different GNP content at 10 MPa in (a) axial, and (b) lateral direction.

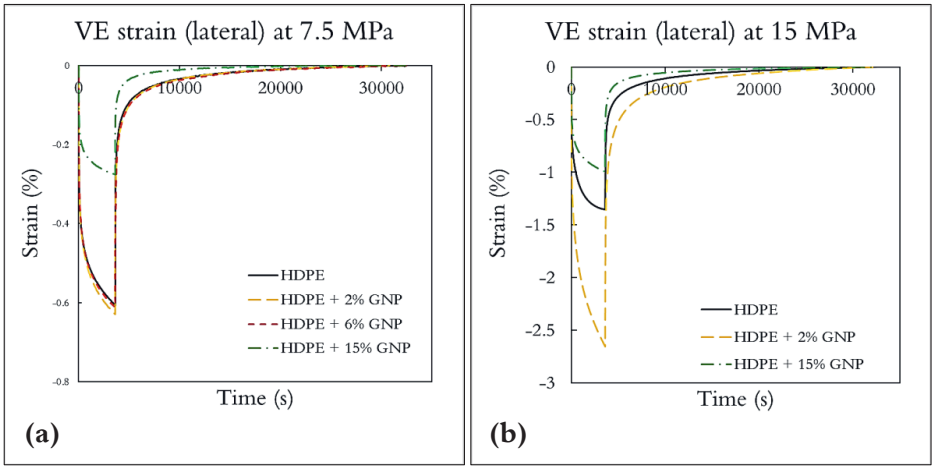

Figure 10. Pure VE strain in lateral direction HDPE with different GNP content at (a) 7.5 MPa and (b) 15 MPa. Data for HDPE+6% GNP are missing due to failure of strain gauge at higher strains.

5. Conclusions

The short creep tests were performed on HDPE doped with various amounts of GNP to characterize viscoplastic properties of these materials and to evaluate effect of nano-reinforcement on VP parameters. The results showed that applied methodology and models can be successfully used to describe non-linear behavior of nano-composites. It was observed that addition of 2 wt% GNP and 6 wt% GNP did not show any significant effect on VP properties. Small changes were observed when 2 wt% of GNP has been added for 12.5 MPa stress level. However, data for the nano-composite with 6wt% of reinforcement at high stress level are somewhat unstable, possibly due to the defect (void) in the material. It is also indicated by the fact that specimen with 6 wt% GNP failed prematurely at 12.5 MPa (thus experimental data for this material were limited).

The most significant difference has been observed with addition of 15 wt% GNP – the VP strain decreases 2 times with respect to neat HDPE at the same loading duration and stress level. These changes were seen for both axial and lateral directions. The VP parameter which characterizes VP strain development with time, is relatively stable for different amount of GNP for axial and lateral direction (except for lateral direction for addition of 6 wt% GNP).

From previous studies it has been observed, that experimental data at higher stresses is crucial for accurate VP parameter identification. The parameters responsible for VP behavior changes with stress, showed significant difference with addition of GNP.

The analysis of viscoelasticity showed similar trend – addition of 15 wt% GNP decreases VE strain more than 2 times (compare to neat HDPE) at the same stress and loading duration. The compliance curves showed that all materials in axial direction exhibit nonlinear viscoelasticity even at very low stress levels (below 10 MPa). The pure HDPE showed only linearly VE behavior and HDPE with 2 wt% GNP showed nonlinear VE behavior at 15 MPa.

Acknowledgments

Part of this study was financially supported by Interreg Nord project "Smart WPC" (funded by EU and Region Norrbotten). Authors would like to thank Runar Långström and Robert Westerlund at RISE SICOMP for composites processing and the help from Diego Carrasco Fernández (project student at LTU) in performing the creep experiment.

References

[1] X. Zhao, Q. Zhang, D. Chen, P. Lu, Enhanced mechanical properties of graphene-based polyvinyl alcohol composites, Macromolecules. 43 (2010) 2357–2363. doi:10.1021/ma902862u.

[2] R.D. Maksimov, J. Bitenieks, E. Plume, J. Zicans, R. Merijs Meri, The effect of introduction of carbon nanotubes on the physicomechanical properties of polyvinylacetate, Mech. Compos. Mater. (2010). doi:10.1007/s11029-010-9142-1.

[3] J. Zicans, R. Merijs Meri, M. Kalniņš, R. Maksimovs, J. Jansons, Modeling and experimental investigations of elastic and creep properties of thermoplastic polymer nanocomposites, ZAMM Zeitschrift Fur Angew. Math. Und Mech. (2015). doi:10.1002/zamm.201400288.

[4] O. Starkova, J. Yang, Z. Zhang, Application of time-stress superposition to nonlinear creep of polyamide 66 filled with nanoparticles of various sizes, Compos. Sci. Technol. (2007). doi:10.1016/j.compscitech.2007.02.014.

[5] X. Shuang, L. Xiaobing, W. Jianfeng, K. Ze, C. Hong, F. Wenxin, L. Zhibo, Role of poly(ethylene glycol) grafted silica nanoparticle shape in toughened PLA-matrix nanocomposites, Compos. Part B Eng. 168 (2019) 398–405.

[6] M. Vakilifard, M.J. Mahmoodi, Dynamic moduli and creep damping analysis of short carbon fiber reinforced polymer hybrid nanocomposite containing silica nanoparticle-on the nanoparticle size and volume fraction dependent aggregation, Compos. Part B Eng. (2019). doi:10.1016/j.compositesb.2018.12.045.

[7] O. Starkova, S.T. Buschhorn, E. Mannov, K. Schulte, A. Aniskevich, Creep and recovery of epoxy/MWCNT nanocomposites, Compos. Part A Appl. Sci. Manuf. (2012). doi:10.1016/j.compositesa.2012.03.015.

[8] S.S.R. Nomula, D.K. Rathore, B.C. Ray, R.K. Prusty, Creep performance of CNT reinforced glass fiber/epoxy composites: Roles of temperature and stress, J. Appl. Polym. Sci. (2019). doi:10.1002/app.47674.

[9] A. Muliana, Nonlinear viscoelastic-degradation model for polymeric based materials, Int. J. Solids Struct. (2014). doi:10.1016/j.ijsolstr.2013.09.016.

[10] M.K. Hassanzadeh-Aghdam, M.J. Mahmoodi, R. Ansari, Creep performance of CNT polymer nanocomposites -An emphasis on viscoelastic interphase and CNT agglomeration, Compos. Part B Eng. (2019). doi:10.1016/j.compositesb.2018.12.093.

[11] L.-C. Tang, X. Wang, L.-X. Gong, K. Peng, L. Zhao, Q. Chen, L.-B. Wu, J.-X. Jiang, G.-Q. Lai, Creep and recovery of polystyrene composites filled with graphene additives, Compos. Sci. Technol. 91 (2014) 63–70. doi:10.1016/J.COMPSCITECH.2013.11.028.

[12] L.J. Zapas, J.M. Crissman, Creep and recovery behaviour of ultra-high molecular weight polyethylene in the region of small uniaxial deformations, Polymer (Guildf). (1984). doi:10.1016/0032-3861(84)90267-2.

[13] L.O. Nordin, J. Varna, Nonlinear viscoplastic and nonlinear viscoelastic material model for paper fiber composites in compression, Compos. Part A Appl. Sci. Manuf. (2006). doi:10.1016/j.compositesa.2005.02.015.

[14] E. Marklund, J. Varna, L. Wallström, Nonlinear Viscoelasticity and Viscoplasticity of Flax/Polypropylene Composites, J. Eng. Mater. Technol. (2006). doi:10.1115/1.2345444.

[15] L. Rozite, J. Varna, R. Joffe, A. Pupurs, Nonlinear behavior of PLA and lignin-based flax composites subjected to tensile loading, J. Thermoplast. Compos. Mater. (2013). doi:10.1177/0892705711425846.

[16] L. Pupure, J. Varna, R. Joffe, On viscoplasticity characterization of natural fibres with high variability, Adv. Compos. Lett. (2015).

[17] K. Giannadakis, J. Varna, Analysis of nonlinear shear stress-strain response of unidirectional GF/EP composite, Compos. Part A Appl. Sci. Manuf. (2014). doi:10.1016/j.compositesa.2014.03.009.

[18] Z. Al-Maqdasi, G. Gong, R. Joffe, Wood Fiber Composites With Added Multi-functionality, 18th Eur. Confernece Compos. Mater. ECCM18. (2018).

[19] Y.C. Lou, R.A. Schapery, Viscoelastic Characterization of a Nonlinear Fiber-Reinforced Plastic, J. Compos. Mater. (1971). doi:10.1177/002199837100500206.

[20] R. Schapery, Further development of a thermodynamic constitutive theory : stress formulation., Purdue Research Foundation, Lafayette, 1969.

[21] R.A. Schapery, On the characterization of nonlinear viscoelastic materials, Polym. Eng. Sci. (1969). doi:10.1002/pen.760090410.

Notes

Department of Engineering Sciences and Mathematics
Division of Materials Science

ISSN 1402-1757
ISBN 978-91-7790-372-7 (print)
ISBN 978-91-7790-373-4 (pdf)

Luleå University of Technology 2019

LULEÅ
UNIVERSITY
OF TECHNOLOGY